A RAMAN SPECTROSCOPIC AND COMPUTATIONAL STUDY ON THE EFFECTS OF ELECTRON WITHDRAWING GROUPS ON HALOGEN BONDING

By:

Katelyn Allen

A thesis submitted to the faculty of The University of Mississippi in partial fulfillment of the requirements of the Sally McDonnell Barksdale Honors College

Oxford
May 2017

Approved By:

_____

Advisor: Professor Nathan Hammer

_____

Reader: Professor Davita Watkins

_____

Reader: Professor Susan Pedigo

ACKNOWLEDGEMENTS

First, I would like to thank my parents Shawn and Heidi Allen, and my brothers Cary and Shawn Michael Allen for supporting me throughout my academic career. Throughout my time at the University of Mississippi several people have relentlessly supported me in every endeavor and challenged me to become a better student, researcher, and person. I would like to thank these people for the lasting impact they have made upon my life. I would also like to thank the members of the Hammer Lab Research Group, specifically Louis McNamara, Sarah Sutton, Lemuel Tsang, and Ashley Williams for their invaluable input and support throughout the course of this research. I would like to thank Suong Nguyen for synthesizing the molecules studied herein, as well as Dr. Davita Watkins for her instrumental role in the project. I would like to thank Thomas Ellington for not only providing computational details critical to this work, but also for mentoring me in all things over the course of the project. Additionally, I would like to thank the Sally McDonnell-Barksdale Honors College for the extraordinary opportunities they have afforded me throughout my time as an undergraduate. Lastly, I extend my deepest gratitude to my research advisor, Dr. Nathan Hammer for recognizing my passion for chemistry, guiding both my undergraduate academic and research careers, and encouraging me to pursue the more challenging opportunity.

ABSTRACT

KATELYN ELIZABETH ALLEN: A Raman Spectroscopic and Computational Study on the Effects of Electron Withdrawing Groups on Halogen Bonding

(Under the direction of Dr. Nathan Hammer)

Here, the effects of individual electron withdrawing groups on halogen bond strength are investigated using Raman spectroscopy and electronic structure calculations. Halogen bonding is a unique and relatively unexplored noncovalent interaction that has recently garnered considerable attention due to its applications in materials development. When a halogen, such as chlorine, bromine, or iodine, accepts electron density from a Lewis base such as the nitrogen of pyridine a halogen bond arises. The anisotropic distribution of electron density about a covalently bound halogen, also known as the σ-hole, plays a significant role in halogen bond formation. The magnitude of the electropositive region increases from chlorine < bromine < iodine. Using a combination of Raman spectroscopy and computational chemistry, eight halogen bond donors with four unique electron withdrawing moieties were evaluated for use as potential molecular building blocks in organic optoelectronic devices. First, the C-I stretches of the ten monomers were assigned using experimental Raman spectra in junction with computed Raman frequencies and activities. The C-I stretch was tracked as a function of electron withdrawing moiety, producing trends that directly connected donor strength to molecular structure. The observation of a red shift in the C-I stretch of the halogen bond donor suggested an electrostatically stronger σ-hole and thus a greater binding energy with halogen bond acceptors. Additionally the C-I stretch, in twelve co-crystals synthesized from promising donors and acceptors, was assigned and tracked. The change in the C-I stretch for the co-crystals was similar to that of the monomers. With this, the change in the C-I stretch as a function of complexation was determined by comparing the C-I stretch of the monomeric halogen bond donor with the C-I stretch of the halogen bond complex. The trend observed agreed with that of the C-I stretch within both the monomer and co-crystal systems. Interestingly, the results of this project suggest that although the σ-hole present on the halogen plays a large role in halogen bond formation, the concentrated belt of electron density surrounding the halogen also significantly contributes to halogen bond strength as well as the vibrational characterization of the molecule.

Table of Contents

LIST OF FIGURES AND TABLES

Chapter 1: Noncovalent Interactions and Halogen Bonding

1.1 Noncovalent Interactions

In nature, chemical bonds occur due to the interaction between positive and negative particles, also known as protons and electrons, which constitute an atom. Two classes of such an interaction are referred to as ionic and covalent bonds.[1] Ionic bonds occur between a metal and a nonmetal and involve the complete transfer of an electron, generally from the metal to the nonmetal. Covalent bonds on the other hand are formed between two nonmetals and involve the sharing of an electron. These bonds are formed because the potential energy is lowered as isolated atoms come together. Additionally, molecular forces allow separated molecules, or monomers, to interact, which can result in the formation of intermolecular dimers provided the energy is lowered upon complexation. These interactions are normally referred to as noncovalent interactions and are considered to be much weaker than both covalent and ionic ones.[2] Although individual noncovalent interactions are significantly weaker than covalent or ionic interactions, they are critical for the formation of double stranded DNA, protein folding, the condensed phase, as well as the chemicophysical properties that drive self-assembly processes in molecular systems. Numerous noncovalent interactions exist in nature including, dispersion forces, dipole-dipole forces, ion-dipole forces, ion-induced dipole forces, hydrogen bonding, and halogen

bonding.[3] Molecules can be thought to have clouds of electron density surrounding their individual atoms, with each atom possessing a degree of polarizability based upon its molecular weight and effective nuclear charge. As a consequence of a molecule's polarizability, dispersion or London forces emerge and exist between all interacting molecules.[1] The fluctuation in the electron distribution of a molecule causes instantaneous or temporary dipoles to form within the molecule. These dipoles in turn affect neighboring molecules by inducing other dipoles throughout the molecule until all interacting molecules are slightly attracted to one another. Polar molecules, or molecules containing permanent dipoles due to electronegativity differences between the atoms constituting the molecule, can interact with the permanent dipoles of other polar molecules; thus, these interactions are deemed dipole-dipole interactions. When an ionic molecule, is mixed with a polar molecule, the attraction between the negatively charged ion and the partially positive pole of the polar molecule is referred to as an ion-dipole interaction. Furthermore, ions can induce molecular dipoles in molecules do not have a naturally occurring one. These interactions are known as ion-induced dipole interactions.[2]

Perhaps the most thoroughly investigated noncovalent interaction is hydrogen bonding due to its fundamental role in both understanding the chemical and physical properties of water and its impact on the structure and assembly of biological molecules.[4-8] As illustrated in Figure 1.1.1, hydrogen bonding can occur between a hydrogen and an electronegative region, which is typically an atom such as oxygen, nitrogen, or fluorine.[9] The electronegativity difference between the two atoms results in a partial positive charge on the hydrogen and a partial negative charge on the more electronegative atom; thus, the net attractive force between molecules through the interaction of the partial positive and

partial negative atoms leads to the formation of a hydrogen bond. While induction and dispersion forces contribute to the formation of a hydrogen bond, the attractive interaction arises mostly from electrostatic forces between permanent dipoles of the polar molecules. Of the previously mentioned noncovalent interactions, hydrogen bonding is the strongest with binding energies ranging from –4 to –10 kcal mol^{-1}. For years, hydrogen bonding was thought to be a unique, almost purely electrostatic, noncovalent interaction. However, within the past century a new noncovalent interaction, sharing several characteristics with the hydrogen bond, has emerged and become of great interest, also known as, the halogen bond.[10,11]

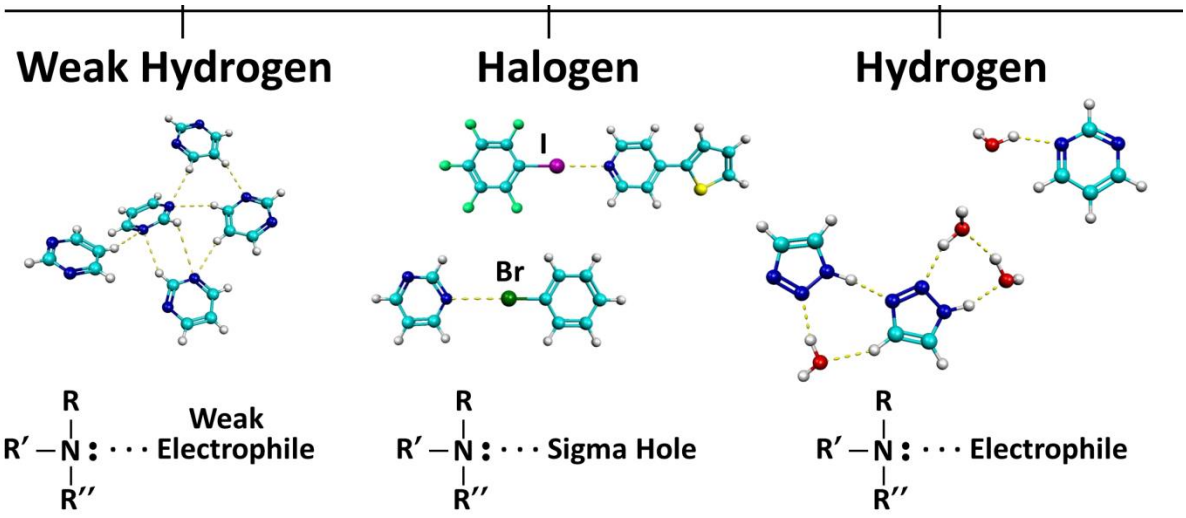

Figure 1.1.1: Range of Noncovalent Interactions

1.2 Halogen Bonding

The first experimental evidence of a halogen bond was reported in 1814, by J. J. Colin under the instruction of J. L. Gay-Lussac, while studying the formation of a metallic liquid after combining dry iodine with gaseous ammonia.[12] However, it would be another 50 years before Guthrie, in his 1863 paper published on iodide of iodoammonium, proposed the structure I_2•••NH_3 for the mixture produced by Colin.[13] This interaction was once again observed in 1896 when Remsen and Norris attempted to synthesize a salt of $SeBr_4(CH_3)_3NHBr$ and accidently created a precipitate completely lacking selenium but concentrated with bromine. This mishap led to the first observations of chlorine and bromine containing complexes acting as electron acceptor species in experiments with several amines.[14] In 1949, Benesi and Hildebrand explained the variety of colors produced when iodine is dissolved in various organic solvents; thus, identifying the first donor-acceptor halogen interactions in solution.[15] Throughout the nineteenth and twentieth centuries scientists unknowingly made unique advancements as a result of the halogen bond. However, it was not until the end of the twentieth century that chemists were able to piece collaborative advancements together and give a name to this highly directional, tunable, noncovalent interaction.[16-18] With the twenty-first century came the realization that halogen bonding had potential for self-assembled adducts through strategic structural design of the molecules involved in the halogen bond formation and interest in halogen bonding significantly grew within the scientific community.[19-21] In 2013, IUPAC set forth the following definition of a halogen bond stating, “A halogen bond occurs when there is evidence of a net attractive interaction between an electrophilic region associated with a halogen atom in a molecular entity and a

nucleophilic region in another, or the same, molecular entity."[22] While halogens are typically thought to be the most electronegative elements and thus possess a partial negative charge, they can accept electron density from a Lewis base such as nitrogen, oxygen, or sulfur as a result of the anisotropic electronic charge distribution around a covalently bound halogen atom.[21,23-25] The polarizability of the halogen gives rise to the region of positive potential, otherwise known as the σ hole, aligned along the covalent bond to the halogen atom, as well as the region of negative potential, known as the belt, around the lateral sides of the halogen atom. Figure 1.2.1 is an electrostatic potential map of the halogen bond donor iodopentafluorobenzene that illustrates the blue electropositive σ-hole as well as the green electronegative belt of electron density that wraps around iodine. Halogen bond strength can be directly correlated to the degree of polarizability associated with the halogen; thus, the strength of the halogen bond increases from fluorine << chlorine < bromine < iodine.[25]

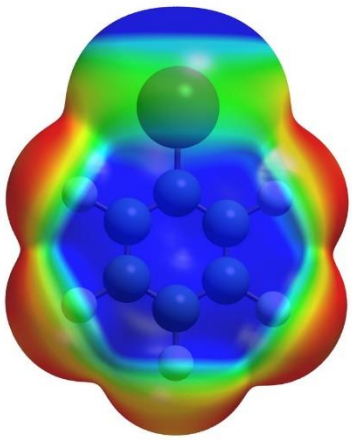

Figure 1.2.1: Electrostatic Potential Map of Iodopentafluorobenzene Optimized using M06-2X/aug-cc-pVDZ-PP

Halogen bonding, previously illustrated in Figure 1.1.1, finds its unique niche in the array of noncovalent interactions in that the strength of halogen bond can be optimized for specific interactions.[20,26] The tunability of the interaction strength can be achieved by manipulating the chemical environment of the molecule via modification of the donor's electron withdrawing moieties and the identity of the halogen atom. It has been extensively demonstrated that stronger electron withdrawing moieties within the halogen bond donor result in a more electropositive sigma hole, consequently resulting in the formation of a stronger halogen bond. Directionality, strength tunability, hydrophobicity, and donor atom dimensions are unique features of the halogen bond which have allowed the interaction to be employed as a routinely used tool in the preparation, design, and development of self-assembled systems. As a result of the potential control over the halogen bond interaction strength, halogen bonding has recently garnered a great deal of interest across multiple disciplines, specifically supramolecular chemistry and crystal engineering.[27]

Previously the Hammer Research Group extensively studied the effects of hydrogen bonding on the normal modes of pyrimidine.[10,28] With a focus on the hydrogen bond acceptor, significant blue shifts in the normal modes ν_1, ν_{6b}, and ν_{8b} of pyrimidine were observed with increased hydrogen bonding. The close relation between hydrogen bonding and halogen bonding subsequently lead to the investigation of the effects of halogen bonding on the normal modes of pyrimidine, where complexation of iodopentafluorobenzene with pyrimidine conveniently revealed a similar blue shift pyrimidine's normal modes to those previously observed in hydrogen bonded pyrimidine systems.[29] Thus, confirming intermolecular interactions such as hydrogen bonding and halogen bonding could be investigated through a combination of vibrational spectroscopy

and electronic structure theory.

Research in crystal engineering and materials science has revealed that noncovalent interactions play crucial roles in controlling the nanoscale architectures as well as enhancing the optoelectronic properties of materials. The properties of supramolecular structures depend not only on the solid-state nanoscale framework of the components but also the molecular building blocks therein, thus a greater understanding of chemical reactivity and self-assembly mechanisms is critical to the enhancement of supramolecular materials.[30,31] Recently, Resnati and coworkers used Far-IR spectroscopy to observe changes in spectral features, specifically the C-I stretch, of liquid iodopentafluorobenzene upon co-crystal formation.[32] With halogen bond formation, a substantial red shift (~12 cm^{-1}) in the C-I stretch of the halogen bond donor iodopentafluorobenzene was observed. However, in their study the characteristic frequencies of the C-I stretches investigated existed in different physical states of matter. As a result, the red shift observed for the C-I stretch upon halogen bond formation may change as a consequence of the sensitivity of normal modes to physical state. In an effort to contribute to the heuristic approach for designing halogen bond donor molecules for use as potential molecular building blocks of optoelectronic materials, herein the C-I stretches of ten halogen bond donors with distinct electron withdrawing moieties are assigned and monitored using Raman spectroscopy and electronic structure theory. In addition, the C-I stretches of twelve co-crystals formed from the most promising halogen bond donors and the thiophene and furan based halogen bond acceptors, are assigned, monitored, and compared to that of the corresponding monomeric halogen bond donor in an effort to better understand how the strength of the halogen bond compares to other intermolecular forces and ultimately the self-assembly mechanisms of

supramolecular materials.

Chapter 2: Spectroscopy

2.1 Definition of Spectroscopy

Spectroscopy in its most broad sense is the interaction between light and matter. This interaction is unique for every molecule as a consequence of the molecule's intrinsic physical and chemical properties.[33] As a result, spectroscopy is a valuable tool for investigating and understanding chemical bonds and reactivity of matter.

2.2 Electromagnetic Radiation

Light, also known as electromagnetic radiation, acts as both a wave and particle; thus, light exhibits what is known as wave-particle duality. In other words, light can not only be described as an oscillating electromagnetic wave containing magnetic and electric field components perpendicular to the direction of propagation, but also as a spatially localized packet of quanta known as a photon.[33] In order to demonstrate this phenomena, Einstein formulated an equation that accurately predicted the relationship between the energy of a photon and the frequency of light.

$$E = h\nu = \frac{hc}{\lambda} \quad (2.2.1)$$

In equation 2.1.1, known as the Planck-Einstein relation, h is defined as Planck's constant with a value of 6.626×10^{-34} J s, ν is the frequency of the light (s^{-1}), c is the speed of light with a value of 3.00×10^{8} m/s, and λ is defined as the wavelength of light (m). From this we see that the energy of a photon is directly proportional to the frequency of the light and

inversely proportional to the wavelength of the light. Thus, demonstrating that a particle can be defined by both frequency and wavelength confirming the wave-particle nature of light. The large frequency and wavelength range of electromagnetic radiation is commonly known as the electromagnetic spectrum found in Figure 2.2.1.

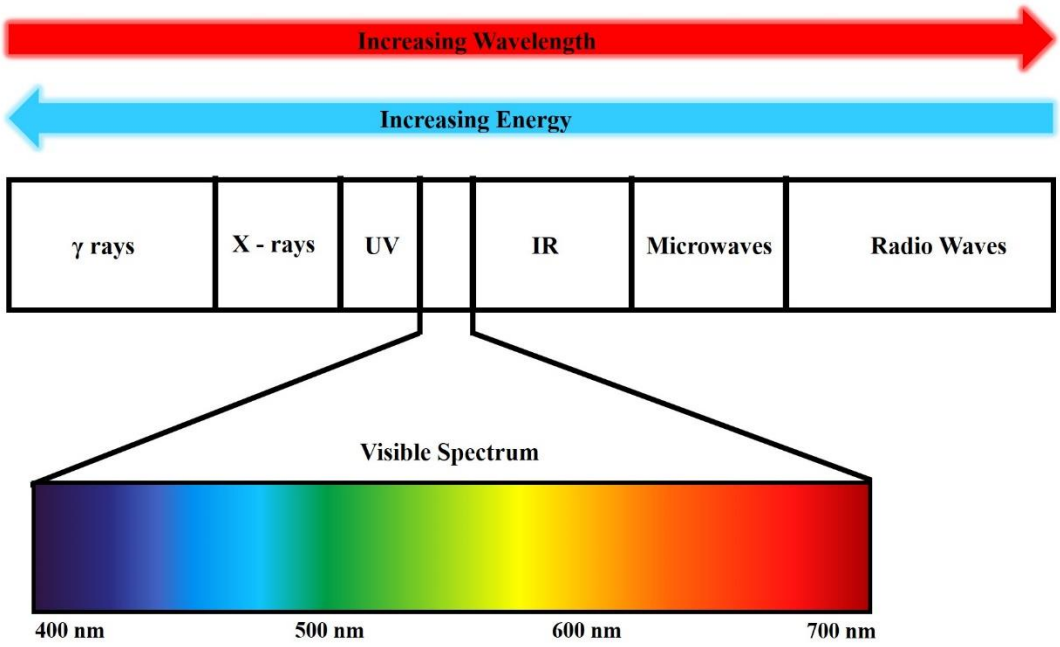

Figure 2.2.1: Electromagnetic Radiation Spectrum

While the visible portion of the electromagnetic spectrum is relatively small, it along with the other regions of the spectrum are incredibly useful for the spectroscopic analysis of molecules. For example, Gamma rays with the highest electromagnetic energy result in the rearrangement of nuclear particles. Subsequently, X-Rays have enough energy to eject core electrons of an atom. The energy of ultraviolet and visible radiation allow for convenient studies of molecular orbitals through the promotion of a valence electron from one electronic state to another. Furthermore, infrared radiation can be used to study molecular vibrations while the microwave region can provide insight into the rotational energy levels of molecules. Finally, the detection of the radio frequencies emitted by nuclei in a magnetic

field allow for the molecular structure of a compound to be determined. Each region of the electromagnetic spectrum has the potential to provide unique, valuable information regarding the physical and chemical properties of molecules.[34]

Spectroscopy is largely based on the principle that molecules possess many different energy states and each region of the electromagnetic spectrum can be associated with a specific type of energetic transition. These transitions can occur by three processes: absorption, spontaneous emission, and stimulated emission. In absorption, an incident photon excites a molecule into a higher energy level. Conversely, during emission a molecule in an excited state emits a photon as it relaxes to a lower energy level. As previously mentioned, two emission processes are possible: spontaneous emission and stimulated emission. Stimulated emission is the emission of photons possessing the same phase and propagation direction as the incident photon. On the other hand, spontaneous emission is a random event that occurs as a function of the lifetime of the excited state and the photons emitted lack uniform phase and propagation direction.[33] Figure 2.2.2 provides an illustration of these three processes in tandem. The red arrows in an upward direction indicate an incident photon while the red arrows with downward direction indicate an emitted photon.

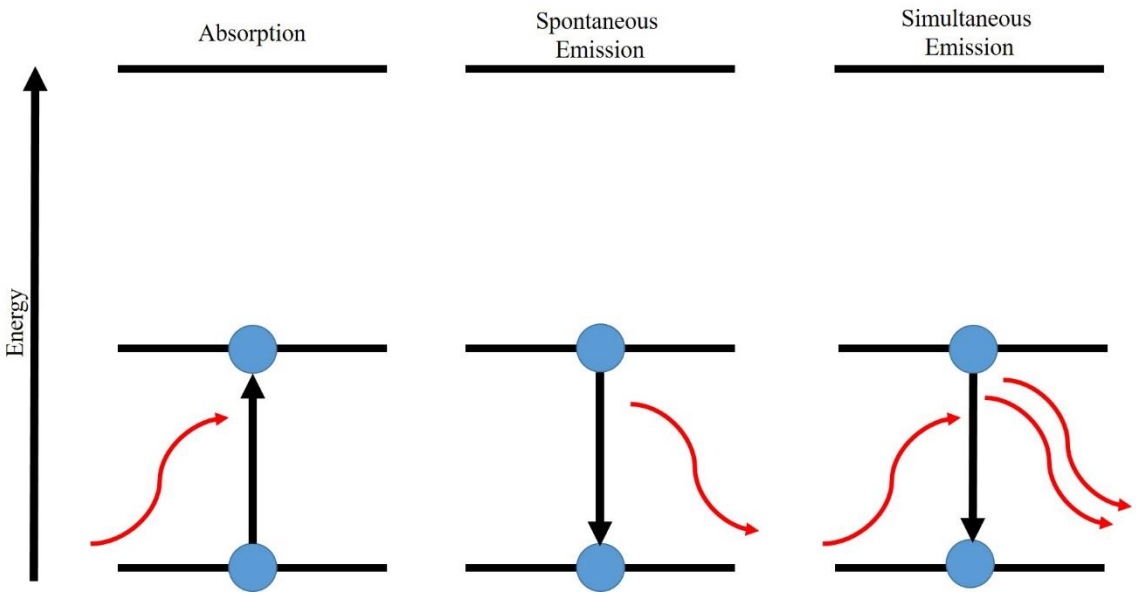

Figure 2.2.2: Absorption, Spontaneous Emission, and Stimulated Emission

Furthermore, these three processes are not independent of each other in a system at equilibrium. Instead, the processes follow Fermi's golden rule which states, the transition rate from the lower energy level to the higher energy level must be equal to the transition rate from the higher energy level to the lower energy level and vice versa.[35] The rates at which these processes occur can be described by the corresponding Einstein coefficients, B_{12} (absorption), B_{21} (stimulated emission), and A_{21} (spontaneous emission). While absorption and stimulated emission are proportional to $\rho(\nu)$, the spectral density as a function of frequency, spontaneous emission is only dependent upon the lifetime of the excited state. Additionally, the rate at which each of these processes occur is dependent upon the molecular population of the state from which each transition occurs. Figure 2.2.3 illustrates these three processes occurring at equilibrium.

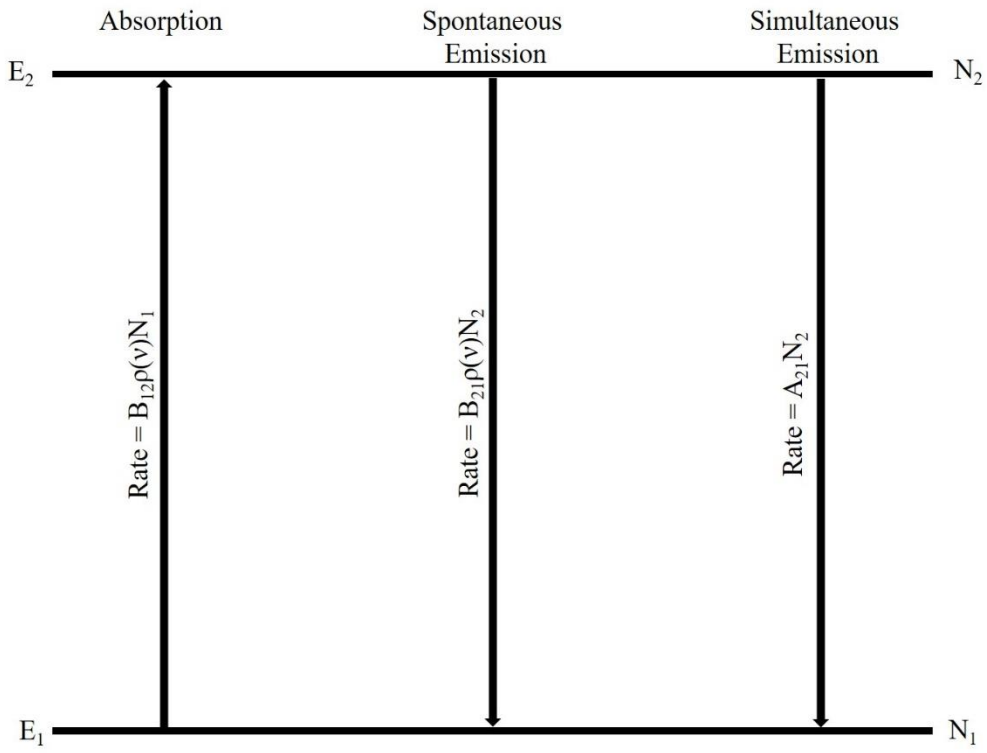

Figure 2.2.3: Einstein Coefficients

For a transition to occur, the starting state of the transition must first be populated. The relative populations of such states, N_1 and N_2, can be calculated using the Maxwell-Boltzmann distribution equation shown in the following equation:

$$\frac{N_2}{N_1} = e^{-(E_2-E_1)/kT} \qquad (2.2.2)$$

Variables E_1 and E_2 correspond to the energy of the transition levels, whereas T corresponds to the temperature of the system in Kelvin and k corresponds to the Boltzmann constant 1.381×10^{-23} JK^{-1}. From this equation, it is possible to determine the population ratio of molecules in the excited state to molecules in the ground state.[33]

Additionally, the rate of absorption must be equal to the sum of both the spontaneous emission and stimulated emission rates as a consequence of systematic equilibrium. Therefore, Einstein rationalized that the ratio of spontaneous emission to stimulated emission must be directly proportionally to the frequency cubed as shown in equation 2.2.3.

$$\frac{A_{21}}{B_{21}} = \frac{8\pi h\nu^3}{\pi c^3} \quad (2.2.3)$$

Ultimately this demonstrated the increasingly competitive relationship between spontaneous and stimulated emission as a function of frequency. This relationship finds significance in that the light emitted by spontaneous emission is incoherent, meaning it does not have a uniform phase nor direction and consequently the intensity of the light diminishes with distance. Conversely, stimulated emission is coherent in that the light emitted is of all the same phase and propagation direction. Therefore, the intensity of the light emitted by stimulated emission is not dependent upon distance. Light bulbs and laser beams are a great examples of incoherent and coherent radiation sources respectively.[33]

2.3 Vibrational Spectroscopy

Vibrational spectroscopy provides unique and significant insight into the nature of a molecule. Because the vibrational frequency of a molecule depends largely on the electronic structure of the atoms involved within the bond and because each vibrational mode occurs at a discrete energy level, vibrational spectroscopy has become an invaluable tool for the characterization of molecular building blocks and their chemicophysical properties.[36,37] A molecular vibration can broadly be characterized as either symmetric or antisymmetric molecular displacement due to the various forces acting on that molecule.

While a stretch is the product of an oscillation about the equilibrium bond length along the axis of the bond, a bend is the product of an oscillation about the equilibrium bond angle. Furthermore, stretches can be characterized as symmetric or antisymmetric and bends can be characterized as a twist, scissor, wag, torque, or rock.[33,35] These motions are illustrated below in Figure 2.3.1.

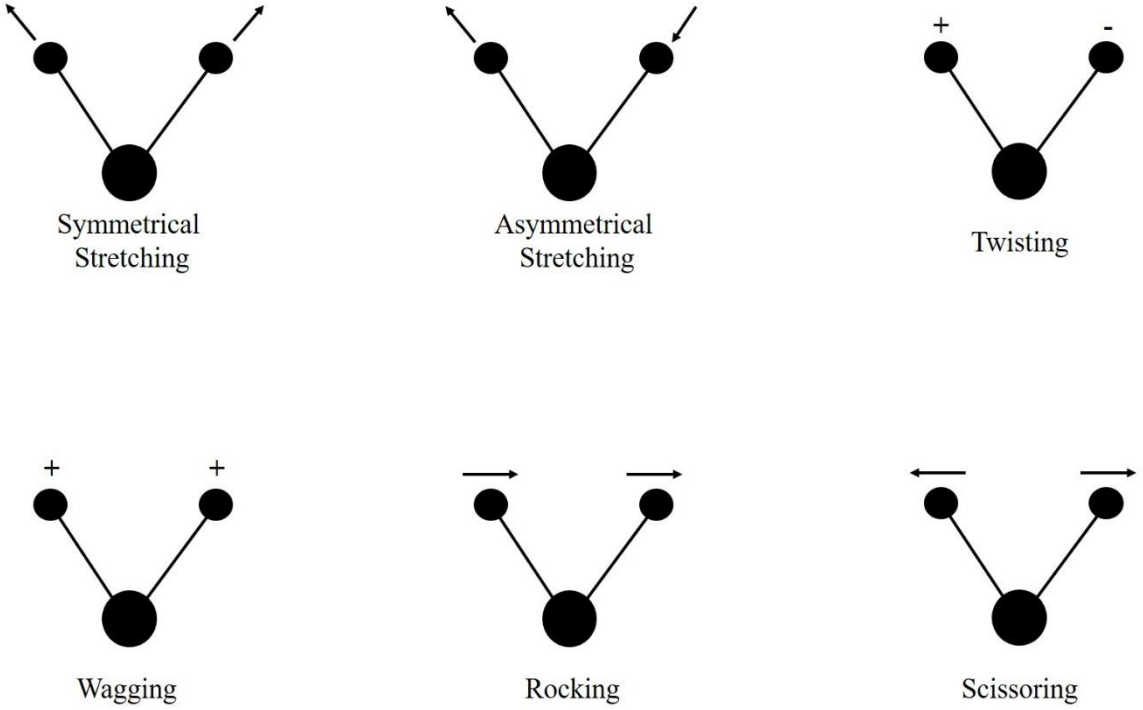

Figure 2.3.1: Possible Vibrational Motions of a Molecule

Additionally, normal modes of vibration occur "where each nucleus executes simple harmonic oscillations about its equilibrium position. All the nuclei move with the same frequency and are in-phase and the center of gravity of the molecule remains unaltered."[36] The number of theoretical vibrational modes can be calculated based on the number of atoms, with three degrees of motion for each atom (i.e., in the x, y, and z directions), and

subtracting out the rotational and translational motions. Based on whether a molecule is linear or not, the number of different vibrational modes varies. Because rotation about the principle molecular axis for a linear molecule cannot be observed, the number of normal vibrational modes can be calculated using the equation 3N-5 while the number of normal vibrational modes for a non-linear molecule can be calculated using the equation 3N-6, where N is equal to the number of atoms within the molecule. Although each vibrational mode corresponds to a peak at a characteristic frequency within a vibrational spectrum, providing valuable insight into a molecule's inherent characteristics, not all theoretical normal modes are observed. This is because some normal modes possess the same energy as others, often referred to as degeneracy. Therefore the mode will not be present in the vibrational spectrum.[33,38]

2.4 The Harmonic Oscillator

In hopes of properly quantifying the vibrational energy levels of a molecule, the quantum mechanical harmonic oscillator and the time-independent Schrödinger equation are employed. In order for a chemical bond to form, a minimum energy must occur. Graphing the potential energy, V(x), as a function of the displacement x from the equilibrium bond length provides insight into how the bond reacts in response to some force. When the atoms are brought close together the electron clouds of the atoms interpenetrate and the slope of the potential exponentially increases. However, increasing the distance between the two atoms results in the asymptote of the curve as the orbital overlap necessary to form a chemical bond approaches zero. Because most molecules occupy only the lowest one or two vibrational energy levels, the functional form of the potential energy near the equilibrium bond length can be approximated by the harmonic

oscillator potential.[33,35,36]

The classical harmonic oscillator is described using a mass connected by a spring to a fixed wall. The spring follows Hooke's law, equation 2.2.4, that states the force on the spring is directly proportional to the displacement of the mass, where F is the force measured, x is the displacement of the mass, and k is the force constant, which is related to the stiffness of the spring.

$$F = -kx \qquad (2.2.4)$$

When x is equal to zero, the system is said to be at equilibrium. The potential energy of the system can be calculated using equation 2.2.5, where k is equal to the force constant of the spring and x is equal to the displacement of the mass.

$$V(x) = \frac{1}{2}kx^2 \quad (2.2.5)$$

The parabolic character of the harmonic potential illustrates the force required for the extension of the spring is equivalent to that required for compression of the spring. However, because the total energy can have any positive value the classic harmonic oscillator has a continuous energy spectrum.[33]

Although equations 2.2.4 and 2.2.5 describe the classical harmonic oscillator and thus classical particles well, they provide only a rough approximation for quantum mechanical particles. Recall that quantum mechanical particles exhibit wave-particle duality. From this, one can clearly see that additional information is needed when attempting to describe quantum mechanical particles; namely, a set of wavefunctions. In this case, the wavefunctions are used to describe the wave-particle nature and molecular vibrations around the equilibrium bond length. As a means to describe said wave functions

and their corresponding vibrational energies, the time-independent Schrödinger equation, as seen in equation 2.2.6, must be solved where μ is the reduced mass (kg), and x is the displacement of the bond length from its equilibrium position (m).

$$-\frac{\hbar^2}{2\mu}\frac{d^2\Psi_n(x)}{dx^2}+\frac{kx^2}{2}\Psi_n(x)=E_n\Psi_n(x) \quad (2.2.6)$$

The solution of the time-independent Schrödinger equation results in a set of normalized wave functions that approach zero for large values of x if the following condition, equation 2.2.7 is met for the eigenvalues, E_n.

$$E_n=h\nu(n+\frac{1}{2}) \qquad (2.2.7)$$

In equation 2.2.7, h is Plank's constant, n is an unique quantum number, and ν is given by equation 2.2.8.

$$\nu=\frac{1}{2\pi}\sqrt{\frac{k}{\mu}} \qquad (2.2.8)$$

The ground state probability density is concentrated at the center of well, implying the particle spends most of its time in this region of the potential. However, as the energy increases the probability density increases at the turning points and coincides with the potential energy of the state. This is demonstrated by both the classical and quantum mechanical harmonic oscillators.[33]

Here, focus is placed on the visible and infrared regions of the electromagnetic spectrum as they are commonly used in various spectroscopic techniques to study the transitions of valence electrons from one vibrational energy level to another higher energy one. The most frequently observed transition occurs between the ground state, v=0, and the

first excited vibrational state, v=1. This is a direct consequence of not only of the higher probability of molecules existing primarily in the ground state as illustrated by the Boltzmann equation but also the selection rules set forth by the quantum mechanical harmonic oscillator. The energy levels and thus transitions between them can be approximated using a potential energy diagram such as the one previously illustrated.

2.5 Selection Rules

Selection rules provide an explanation for the observable transitions that occur between energy levels. Every form of spectroscopy has a set of selection rules which are derived from the transition dipole moment integral, equation 2.2.9, where x is the spatial variable, μ is the dipole moment along the electric field direction, and m and n are two unique vibrational energy levels.[33]

$$\mu_x^{mn} = \int \psi_m^*(x)\mu_x(x_e + x)\psi_n(x)dx \neq 0 \qquad (2.2.9)$$

The direction of the complex vector $\mu_x(x_e + x)$ gives the polarization of the transition and thus determines how the system will interact with an electromagnetic wave of a given polarization. In order for the probability of a transition from state n to m to be nonzero within the harmonic oscillator approximation, the transition dipole moment μ_x^{mn} must be defined in such a way. Consequently, the quantity of vibrational transitions, and thus molecular motions, observed in vibrational spectroscopy relies on not only the number of constituents that make up the molecule but also the molecular motion.

Chapter 3: Raman Spectroscopy Principles and Instrumentation

3.1 Principles of Raman Spectroscopy

Raman spectroscopy is a powerful spectroscopic technique that can be utilized to study the vibrational and rotational energy levels of molecules via light scattering. While Raman spectroscopy and infrared spectroscopy, another spectroscopic technique used to probe molecular vibrational energy levels, are often utilized in tandem to provide a comprehensive evaluation of molecular vibrations unique to specific molecules, the principles upon which each technique is based are vastly different. Infrared spectroscopy selection rules require a net change in the dipole moment of the vibrational mode of the molecule for the molecule to be IR active. Meanwhile, the selection rules of Raman spectroscopy dictate that for a molecule to be Raman active, a net change in the polarizability of the vibrational mode of the molecule must occur.[33,36,38-40] Each normal vibrational mode of an asymmetric molecule demonstrates both a net change in the dipole moment and polarization of the molecule during vibration. Thus, asymmetric molecules are both IR and Raman active. However, the mutual exclusion rule applies for molecules possessing a center of symmetry. The mutual exclusion rule states that for symmetric molecules, the normal vibrational modes observed in the IR spectra will not be observed in the Raman spectra and vice versa. In other words, a net change will not occur in the dipole oment during a symmetric stretch of a symmetric molecule, but a net change will

occur in the polarizability of the molecule. Therefore, symmetric vibrational modes generally exhibit large Raman activities while asymmetric modes exhibit small, if any, Raman activity. In contrast, asymmetric vibrational modes demonstrate large infrared activities while symmetric vibrational modes do not. Hence the complementary relationship between the two techniques.

Raman spectroscopy employs a laser, as a monochromatic, coherent light source, for the excitation of molecules to a virtual energy level. Upon relaxation of the molecule from the virtual state, light is scattered in one of three manners illustrated in Figure 3.1.1.

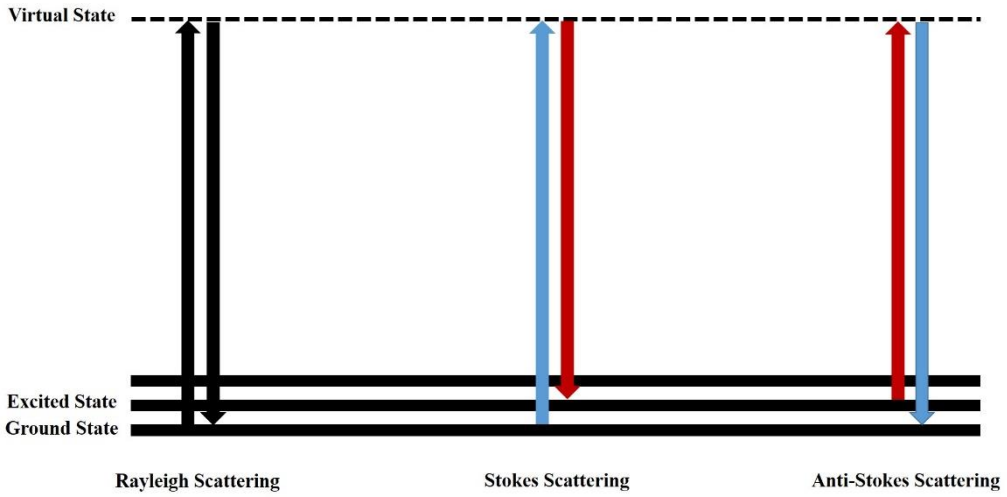

Figure 3.1.1: Rayleigh, Stokes, and Anti-Stokes scattering

In Rayleigh scattering, the incidence radiation interacts with a molecule and the light scattered by the molecule is of the same wavelength as the incident radiation; thus, Rayleigh scattering is an elastic process. Conversely, in Raman scattering the incident radiation interacts with a molecule and the incident radiation can either transfer energy to or gain energy from the interaction with the molecule. While the vast majority of light is Rayleigh scattered, one in every million photons interacts inelastically with matter. Stokes

scattering occurs when the incident photon transfers energy to the molecule, resulting in the promotion of the molecule to a higher vibrational state and the scattered photon possessing a longer wavelength and lower energy than the incident photon. In contrast, anti-stokes scattering occurs when a molecule in an excited vibrational energy state transfers energy to the incident photon, resulting in the relaxation of the molecule to a lower vibrational energy level and the scattered photon possessing a shorter wavelength and higher energy than that of the incident photon. The vibrational frequency of the light scattered by the molecule is thus measured as a shift from the vibrational frequency of the incident radiation. At room temperature, the probability of molecules occupying the ground vibrational state is significantly higher than that of the probability of molecules occupying an excited vibrational state. Consequently, the signal produced by anti-stokes scattered photons is significantly weaker than that of the signal produced by stokes scattered photons. However as a consequence of the law of conservation of energy, stokes and anti-stokes scattering occurs at the same frequencies on either side of the incident radiation frequency. Seeing as the same information can be gathered from both forms of scattering, and stokes scattering is more readily observable, stokes scattering is primarily utilized in Raman analysis.[39,40]

Finally, a change in the frequency at which a vibrational mode is normally observed is referred to as a shift. For historical reasons, a shift to higher energy is referred to as a blue shift while a shift to lower energy is referred to as a red shift. Blue shifts and red shifts are commonly utilized to describe the frequency changes for normal vibrational modes across spectra.[33]

3.2 Raman Spectroscopy Instrumentation

The most basic Raman spectrometer requires an excitation source, sample optics, sample holder, monochromator, and detection system. A box diagram for a basic Raman set up is shown in Figure 3.2.1.

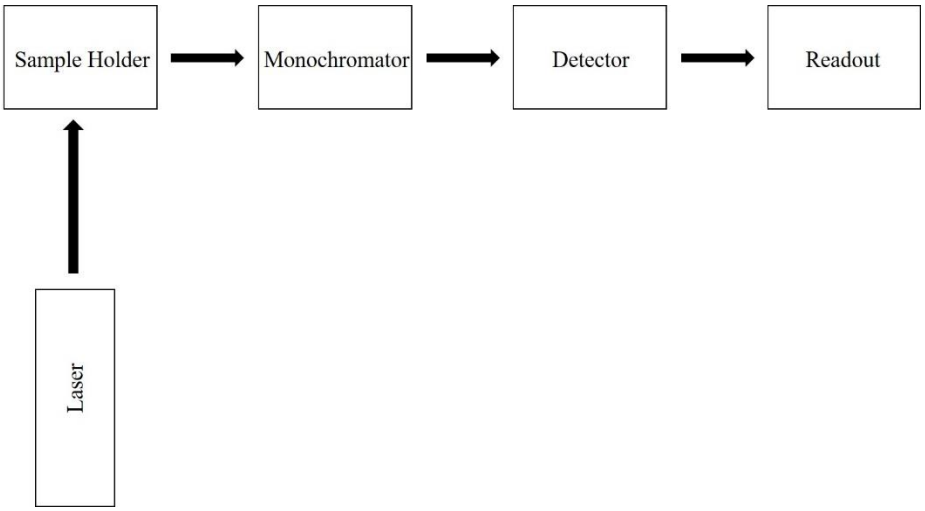

Figure 3.2.1: Basic Box Diagram of a Raman spectrometer

Unlike infrared spectroscopy, which utilizes a continuous radiation source, Raman spectroscopy requires a monochromatic, coherent source such as a laser. The high power, small beam diameter, and polarized character of a laser make it an ideal excitation source for Raman spectroscopy. Lasers function on the principle of population inversion. When a system is at thermal equilibrium, the Maxwell-Boltzmann distribution law (equation 2.2.2) governs the population ratio of molecules in the ground and excited states. As the required energy for a transition increases, the population of the excited state exponentially decreases. Therefore, excited state molecules spontaneously emit photons and revert to the ground state as a means of maintaining equilibrium. As a consequence of the ground state

consistently being more populated than the excited state, a photon is more likely to be absorbed by a molecule in the ground state rather than stimulate emission from the excited state. For stimulated emission to take place, the population of the excited state must be greater than that of the ground state. Upon population inversion, the spontaneously emitted photons will stimulate the emission of other photons and thus lead to a cascade of emitted photons that not only have the same energy but also the same phase as the original photon. To create a population inversion, a laser medium is combined with a power supply and an optical resonator is utilized to amplify the resulting laser beam; ultimately producing a monochromatic, coherent, high power, stable, excitation source.[33] Various lasers are commercially available and are frequently utilized in Raman spectroscopy. Commonly utilized continuous wave lasers include the Ar^+ (351.1-514.5 nm) laser, Kr^+ (337.4-676.4 nm) laser, and the He-Ne (632.8 nm) laser while the most commonly utilized pulsed lasers include the Nd: YAG laser, diode laser, and excimer laser.[39] However, shorter wavelengths are more lightly to induce fluorescence since more electronic transitions occur in the ultra-violet and visible region of the electromagnetic spectrum than in the infrared region. For this reason, a near infrared (NIR) diode laser with a wavelength of 785.0 nm was utilized in this experiment. Furthermore, despite the highly monochromatic and linearly polarized character of laser beams, bandpass filters and half-wave plates are necessary in order to remove any extraneous wavelengths and ensure complete polarization of the laser beam respectively.

Additionally, dispersive monochromators composed of diffraction gratings are utilized to separate polychromatic light into its monochromatic components and thus ensure optimum spectral resolution. A diffraction grating is simply a highly polished

surface with profuse parallel, uniformly spaced grooves. Deconstructive interference occurs upon light striking the grating to result in the light diffracting into its monochromatic components, which are subsequently projected onto the detector. To collect the different wavelengths of light, the grating is rotated as the instrument scans and thus a spectrum is generated.[41] A silicon *charged coupled device* (CCD) detector will be utilized here because it is equipped with multiple pixels that collect each collect narrow ranges of wavelengths simultaneously and ultimately operates much faster than other detectors commonly used to collect scattered such as a photomultiplier tube.[38]

Moreover, whether the analyte exists as a solid or liquid dictates whether micro- or macro- Raman spectroscopy will be utilized. For solid samples, micro-Raman spectroscopy is typically utilized because the monochromatic, polarized laser beam can be focused on to a microscopic area of the sample using a 100x microscope objective. However, macro-Raman allows for easy analysis of bulk phase samples such as liquids. The monochromatic, polarized laser beam can be passed directly through the cuvette rather than being focused onto a small area. Here, liquid and solid samples are studied therefore both techniques are employed.[40]

Chapter 4: Theoretical Chemistry

4.1 Born-Oppenheimer Approximation

Theoretical chemistry is an area of chemistry that relies on quantum mechanics to provide insight into the electronic structure of atoms and molecules. Using high performance computers, essential information needed for the proper interpretation and rationalization of experimental results is gathered. Although the Schrödinger equation, equation 4.1.1, can only be analytically solved for one-electron systems due to the complexity involved in a 3-body problem, computational chemistry seeks to approximate solutions of the equation for much larger systems using the Born-Oppenheimer approximation.

$$\hat{H}\Psi = E\Psi \quad (4.1.1)$$

Where E is the total energy of the system and Ψ is the *n*-electron wave function that not only depends on positions of the nuclei and on the total number of electrons. $\hat{H}$, Hamiltonian operator, is described by equation 4.1.2, which consists of the kinetic and potential energies for each of the particles in the system of interest.

$$\hat{H} = -\frac{\hbar^2}{2m_e}\sum_i^{electrons}\nabla_i^2 - \frac{\hbar^2}{2}\sum_A^{nuclei}\frac{1}{M_A}\nabla_A^2 - \frac{e^2}{4\pi\varepsilon_0}\sum_i^{electrons}\sum_A^{nuclei}\frac{Z_A}{r_{iA}}$$

$$+\frac{e^2}{4\pi\varepsilon_0}\sum_i^{electrons}\sum_j^{electrons}\frac{1}{r_{ij}} + \frac{e^2}{4\pi\varepsilon_0}\sum_A^{nuclei}\sum_B^{nuclei}\frac{Z_A Z_B}{R_{AB}} \quad (4.1.2)$$

In equation 4.1.2, Z_A is the nuclear charge of nucleus A, M_A is the mass of nucleus A, m_e is the mass of electron, R_{AB} is the distance between nuclei A and B, r_{ij} is the distance between electrons i and j, r_{iA} is the distance between electron i and nucleus A, ε_0 is the permittivity of free space, $\hbar$ is Planck's constant divided by 2π, and ∇_i^2 and ∇_A^2 are the Laplace operators of electron I and nucleus A respectively.

4.2 Computational Methods

In this study, the computational program Gaussian09 was utilized to approximate solutions of the time independent Schrödinger equation for the multielectron systems studied. However, to utilize the Gaussian09 software package, a method and basis set must first be defined. Unlike other methods, density functional theory methods significantly simplify and speed up theoretical analysis of various systems by essentially considering the electron density (ρ) rather than explicit e^--e^- interactions. Surprisingly, despite the drastic decrease in dependencies, methods such as the M06-2X global hybrid density functional utilized here have had great success in the ongoing investigation of ground state electronic structure. Additionally, to describe molecular orbitals of a given complex, a basis set is necessary. A single basis function describes an atomic orbital; therefore a set of basis functions, referred to as a basis set, is a linear combination of atomic orbitals that can be utilized to describe molecular orbitals. Moreover, basis functions can be linearly added together to approach the complete basis set limit while giving a more accurate description of the molecule's electronic structure. To describe the molecular orbitals of the systems investigated here, a double-ζ correlation consistent basis set augmented with diffuse functions on all atoms and a small-core energy-consistent relativistic pseudopotential on

iodine centers (aug-cc-pVDZ-PP) was employed. For the theoretically computed information to be insightful, the optimized geometry of the molecule must first be determined via an optimization calculation. Optimization calculations determined the lowest energy geometrical configuration of a molecule or molecular complex by searching the potential energy surface for a stationary point, or a point at which all forces on the molecule are minimized. The optimized geometry of the system can then be utilized to solve for the specific vibrational frequencies observed at that stationary point. The theoretically determined vibrational frequencies can then be compared to those experimentally observed and potentially aid in the assignment and understand of various molecular vibrational modes.

Chapter 5: Analysis of Electron Withdrawing Moiety Effects

5.1 Systems of Interest

The ten halogen bond donors investigated are shown in Figure 5.1.1 and the twelve co-crystals of interest are presented in Figure 5.1.2.

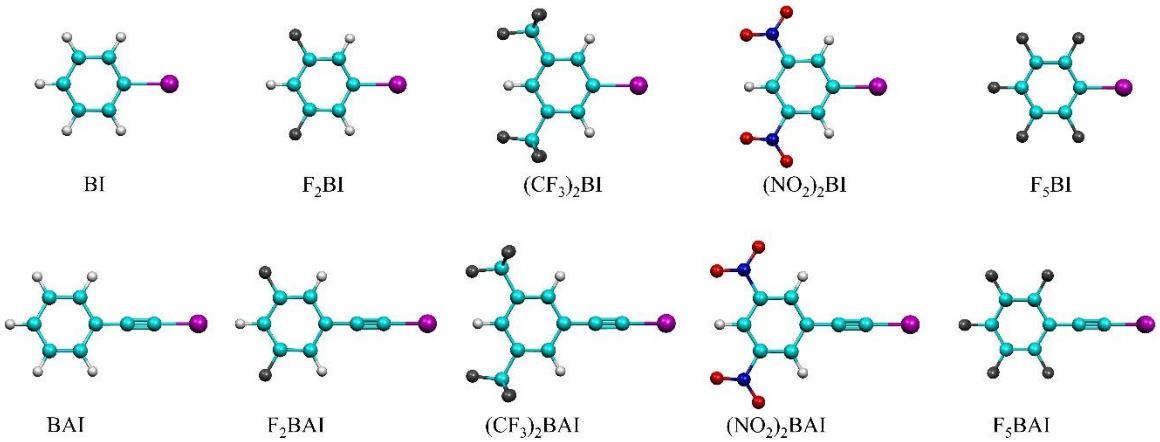

Figure 5.1.1 Monomeric Halogen Bond Donors

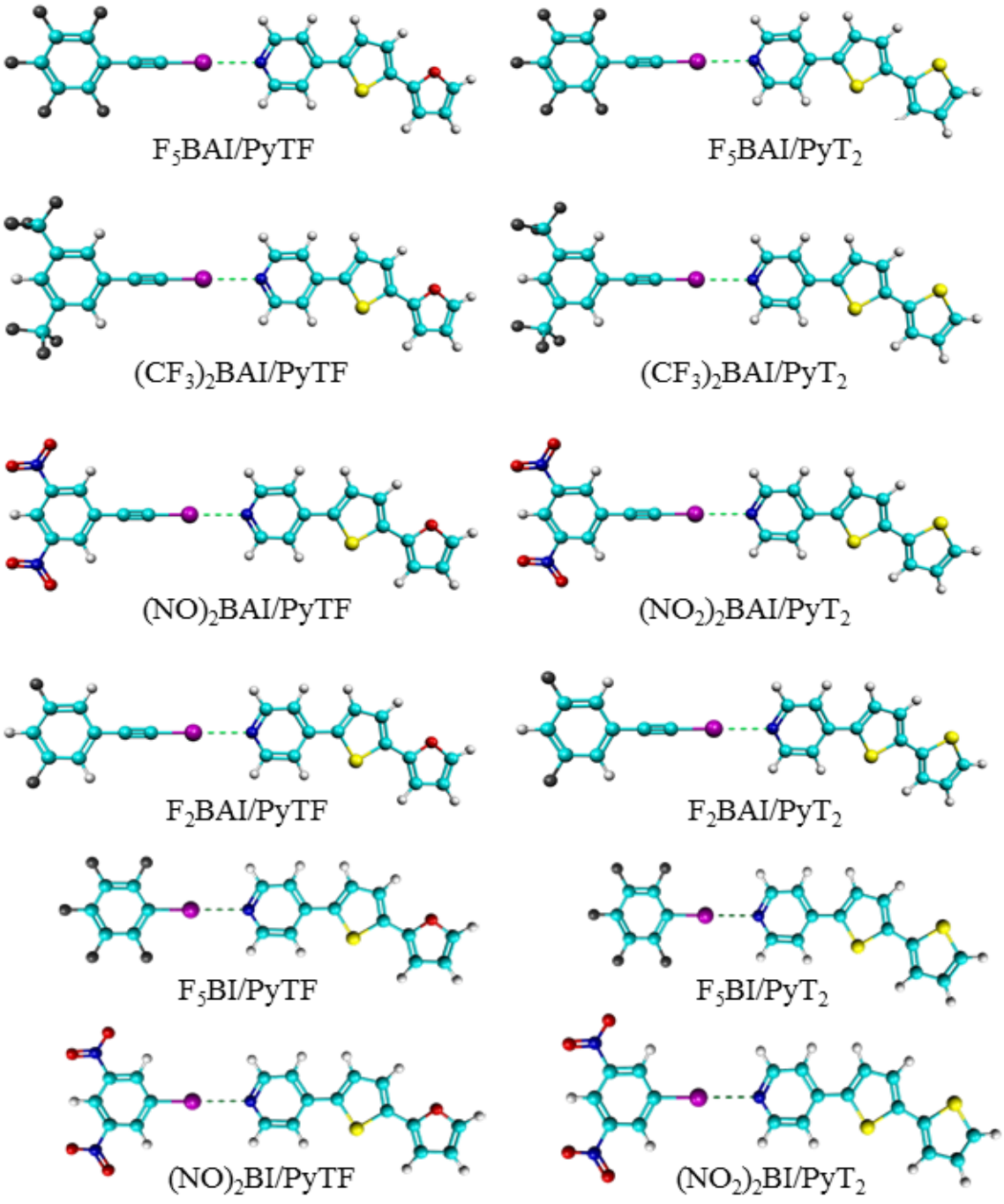

Figure 5.1.2 Co-Crystal Complexes

5.2 Experimental Details

The Horiba Scientific LabRAM HR Evolution Raman Spectroscopy system with CCD camera detection, shown in Figure 5.2.1, was used for the acquisition of solution and solid phase Raman spectra.

Figure 5.2.1: Horiba Scientific LabRAM HR Evolution Raman Spectrometer

The confocal microscope and high throughput 800 mm single stage spectrometer of the LabRAM HR Evolution Raman Spectrometer allows for high-resolution imaging of the co-crystals as well as optimum spectral acquisition of all monomers and co-crystals of interest. Thus, accurate peak assignments were made with a spectral resolution of less than 1 cm^{-1}. The spectrum of each solid sample was optimized by locating a flat, semitransparent section of the sample with high potential for scattering utilizing the motorized stage and video features of the Raman Spectrometer. For liquid samples, a macro-Raman accessory was utilized. Additionally, a Linkam Scientific THMS600 microscope stage was utilized to obtain temperature controlled Raman spectra for all liquid samples. All spectra were obtained using a 785 nm diode laser and a 600 gr/mm diffraction grating.

5.3 Computational Details

Full geometry optimizations and harmonic vibrational frequency computations with IR intensities and Raman activities were performed on the halogen bond donors, acceptors, and their corresponding complexes using the global hybrid M06-2X[1] density functional in conjunction with a double-ζ correlation consistent basis set augmented with diffuse functions on all atoms and a small-core energy-consistent relativistic pseudopotential on iodine centers (aug-cc-pVDZ-PP).[2-4] Electrostatic potential maps were constructed for each XB donor using a total electron density isosurface value of 0.0004. All computations were performed using the analytic gradients and Hessians available in the Gaussian09 software package.[6] Here, only the necessary calculations for assigning the C-I stretch in halogen bond donors and their corresponding complexes are presented; however, it should be noted analysis of the observed trends would not have been possible without the additional calculations absent from this work.

**All computations were performed by Thomas L. Ellington from the Tschumper Research Group

Chapter 6: Monomeric Results and Discussion

Here, the Raman spectra of five iodobenzene and five (iodoethynyl)benzene derivatives seen in Figure 5.1.1 are presented with a focus on the C-I stretching frequency as a method for quantifying halogen bond interaction strengths.

6.1 Effects of Physical State

Over the course of this study it became apparent that it would be necessary to compare Raman spectral features of the same physical state. This is because normal modes are very sensitive to physical state and here it is important to track changes due to halogen bond formation. The spectral features of solids can vary greatly compared to those of liquids due to crystal splitting an other intermolecular interactions not-present in solution. This is especially evident in the Raman spectra of solid and liquid iodopentafluorobenzene illustrated in Figure 6.1.1. Additionally, potential ambiguity in the assignment of the C-I stretch is minimized using both the Raman spectra of the liquid phase and solid phase in conjunction with the theoretical frequency of the C-I stretch.

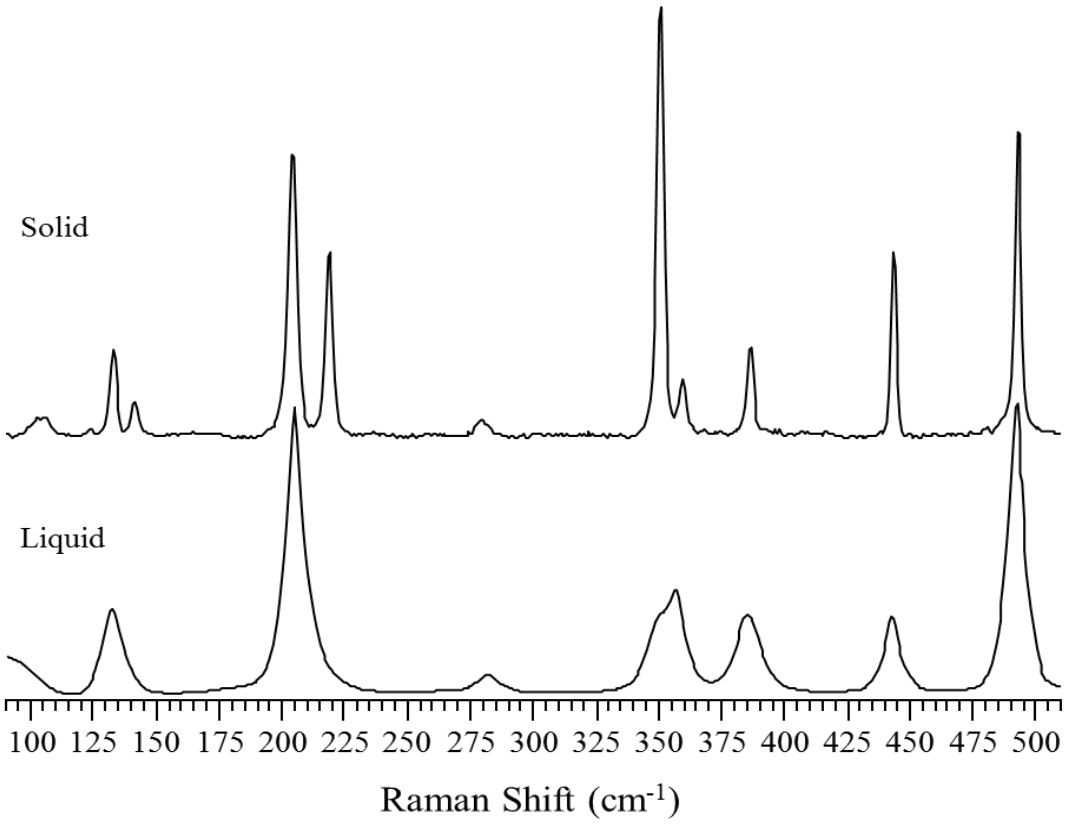

Figure 6.1.1: Effects of Physical State on the C-I stretch of Iodopentafluorobenzene

6.2 Trend in the C-I Stretch for Iodobenzene Derivatives

Comparison of the Raman spectra with the theoretically calculated frequency of the C-I stretch for the five iodobenzene derivatives aided in confident assignment of the C-I stretch in each experimental Raman spectra. Figure 6.1.2 illustrates the agreement seen between the experimental spectra and the theoretically calculated Raman frequencies for the $(NO_2)_2BI$ monomer. Additionally, the experimental and theoretical frequencies of the C-I stretch in each iodobenzene halogen bond donor derivative are reported in Table 6.1.1.

Table 6.2.1: Experimental Raman and Theoretical Frequencies of the C-I Stretches in Iodobenzene Derivatives

	C-I Stretch (cm^{-1})	
XB Donor	**Experiment**	**Theory**
F_5BI	205.07	208.19
$(CF_3)_2BI$	219.50	225.18
F_2BI	230.05	234.20
$(NO_2)_2BI$*	240.50	246.33
BI	266.58	273.52

*$(NO_2)_2BI$ is a solid at room temperature.

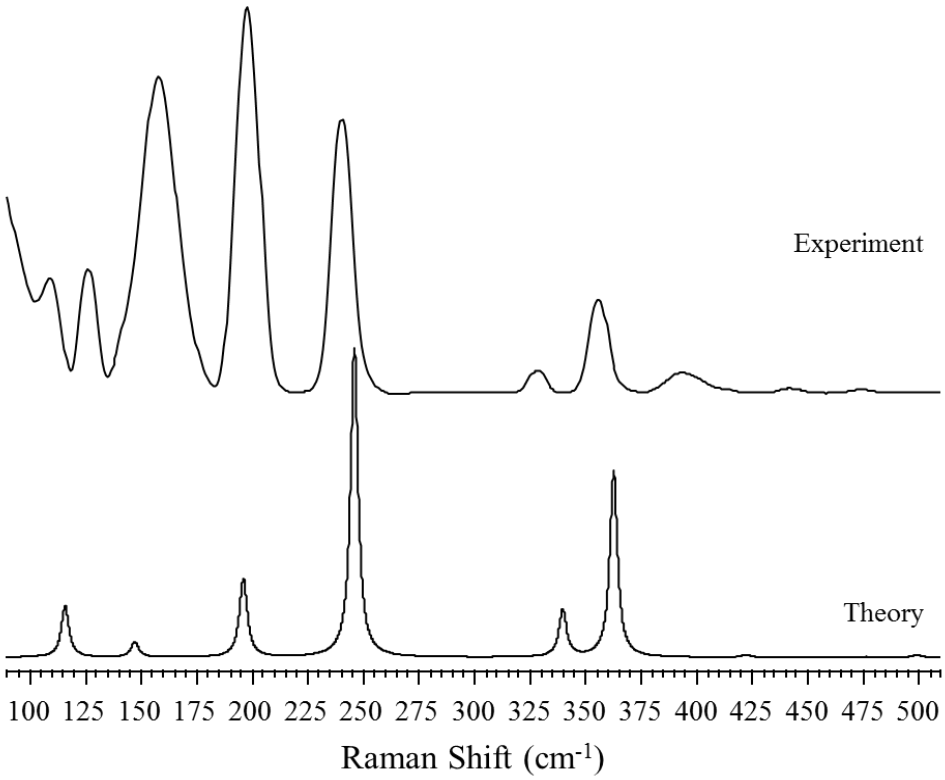

Figure 6.2.1: Agreement between the Experimental Raman Spectra of $(NO_2)_2BI$ and the Theoretically Predicted Raman Spectra

Spectral observations revealed a red shift, a shift to lower energy, in the C-I stretching mode and resulted in the following trend; BI < $(NO_2)_2$BI < $(F_2)_2$BI < $(CF_3)_2$BI < F_5BI, with the C-I stretching mode being the furthest red shifted in F_5BI. This trend is presented in Figure 6.2.3.

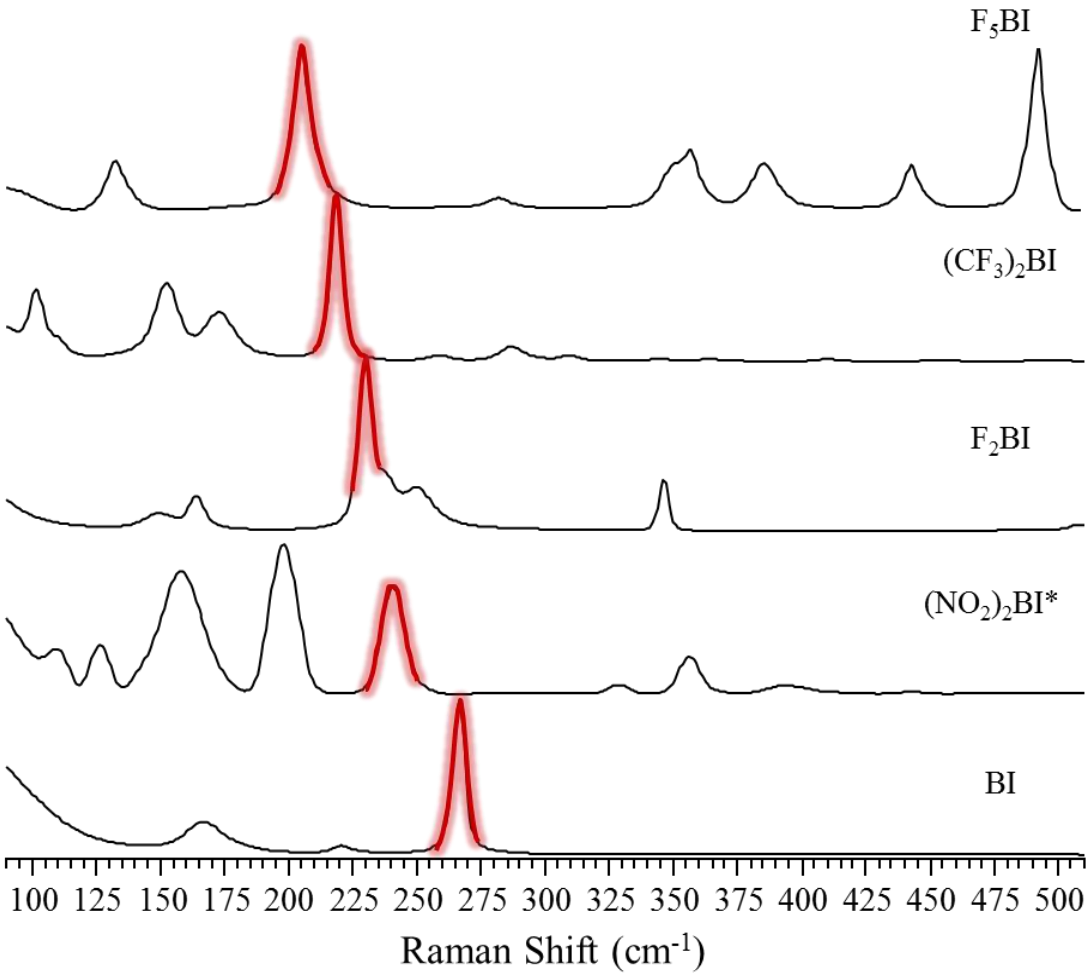

Figure 6.2.3: Trend in the C-I Stretch Observed in the Raman Spectra for Iodobenzene XB Donor Derivatives

The observation of a red shift, a shift to lower energy, implies a decrease in intramolecular bond strength and thus an increase in the intermolecular bond strength (i.e. the halogen bond).[5,42] Great focus has been previously placed on the electron withdrawing moieties of halogen bond donors, resulting in the general consensus that as the electron withdrawing power of the moiety increases the electropositive magnitude of the σ-hole on the halogen increases, and therefore results in the formation of a stronger halogen bond as a consequence of stronger electrostatic forces between the halogen bond donor and acceptor.[11,20,21,25,43,44] However, the results presented here suggest that a delicate balance exists between the electron withdrawing moieties, electropositive magnitude of the σ-hole, and the electronegative belt perpendicular to the C-I bond when attempting to optimize and characterize halogen bonding interactions.

6.3 Trend in the C-I Stretch for (Iodoethynyl)benzene Derivatives

In addition, five complementary (iodoethynyl)benzene derivatives were analyzed to observe the trend in the stretching frequencies of the C-I bond with varying electron withdrawing groups as well speculate how the C-I stretching frequencies changed as a hybridization function of the carbon involved in the C-I bond.

Comparison of the Raman spectra with the theoretically calculated frequency of the C-I stretch for the (iodoethynyl)benzene derivatives aided in confident assignment of the C-I stretch in each Raman spectra. Figure 6.2.1 illustrates the agreement seen between the experimental Raman spectra and the theoretically calculated Raman frequencies for

$(NO_2)_2$BAI. Additionally, the experimental and theoretical frequencies of the C-I stretch in each (iodoethynyl)benzene halogen bond donor derivative are reported in Table 6.2.1.

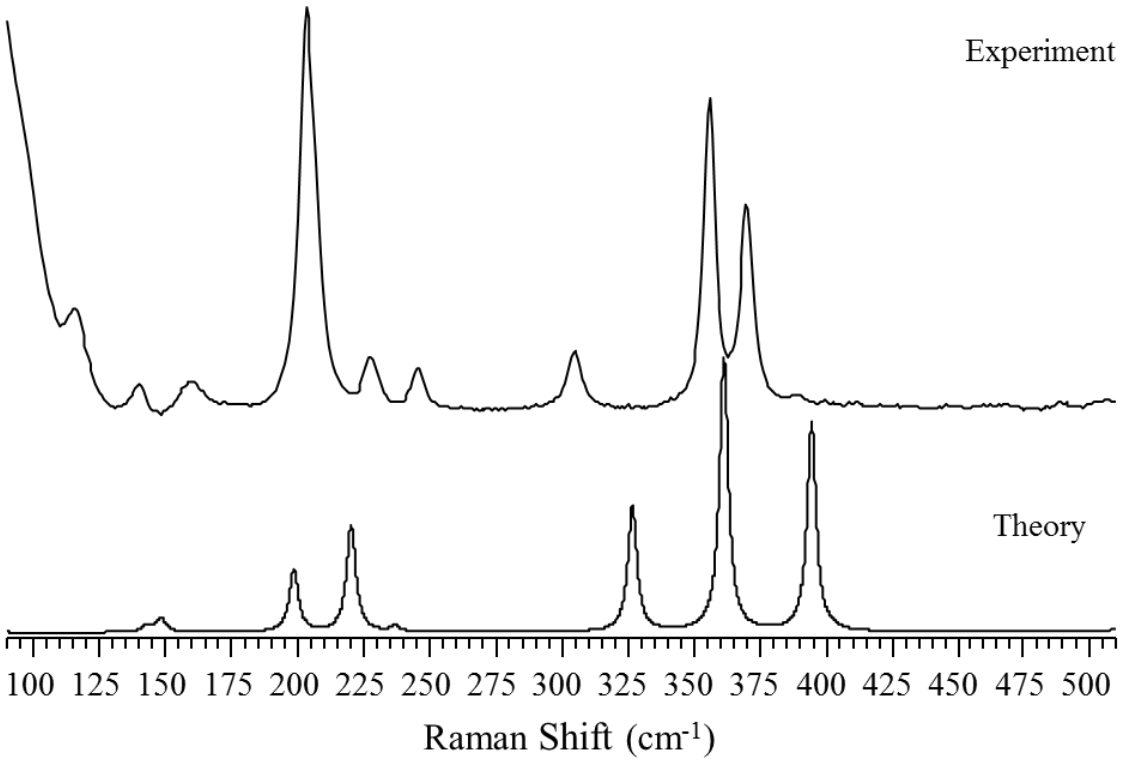

Figure 6.3.1: Agreement between the experimental Raman spectra of $(NO_2)_2$BAI and the theoretically predicted Raman spectra

Table 6.3.1 Experimental Raman and Theoretical Frequencies of the C-I stretches in (iodoethynyl)benzene derivatives

	C-I Stretch (cm^{-1})	
XB Donor	**Experimental**	**Theory**
F_5BAI	178.47	179.19
$(CF_3)_2$BAI	197.86	201.61
$(NO_2)_2$BAI*	203.22	219.85
F_2BAI	207.22	206.19
BAI	238.24	236.45

*$(NO_2)_2$BAI is a solid at room temperature.

Spectral observations revealed a red shift, a shift to lower energy, in the C-I stretching mode and, as expected, resulted in a similar trend to that of the complementary iodobenzene derivatives; BAI < F_2BAI <$(NO_2)_2$BAI < $(CF_3)_2$BAI < F_5BAI, with the C-I stretching mode being the furthest red shifted in F_5BAI. Furthermore suggesting the electropositive magnitude of the σ-hole plays a smaller role in halogen bond strength than previously thought. The trend in the C-I stretching frequency of the five (iodoethynyl)benzene halogen bond donor derivatives is presented in Figure 6.2.2 and the individual Raman spectra of each derivative may be found in the appendix.

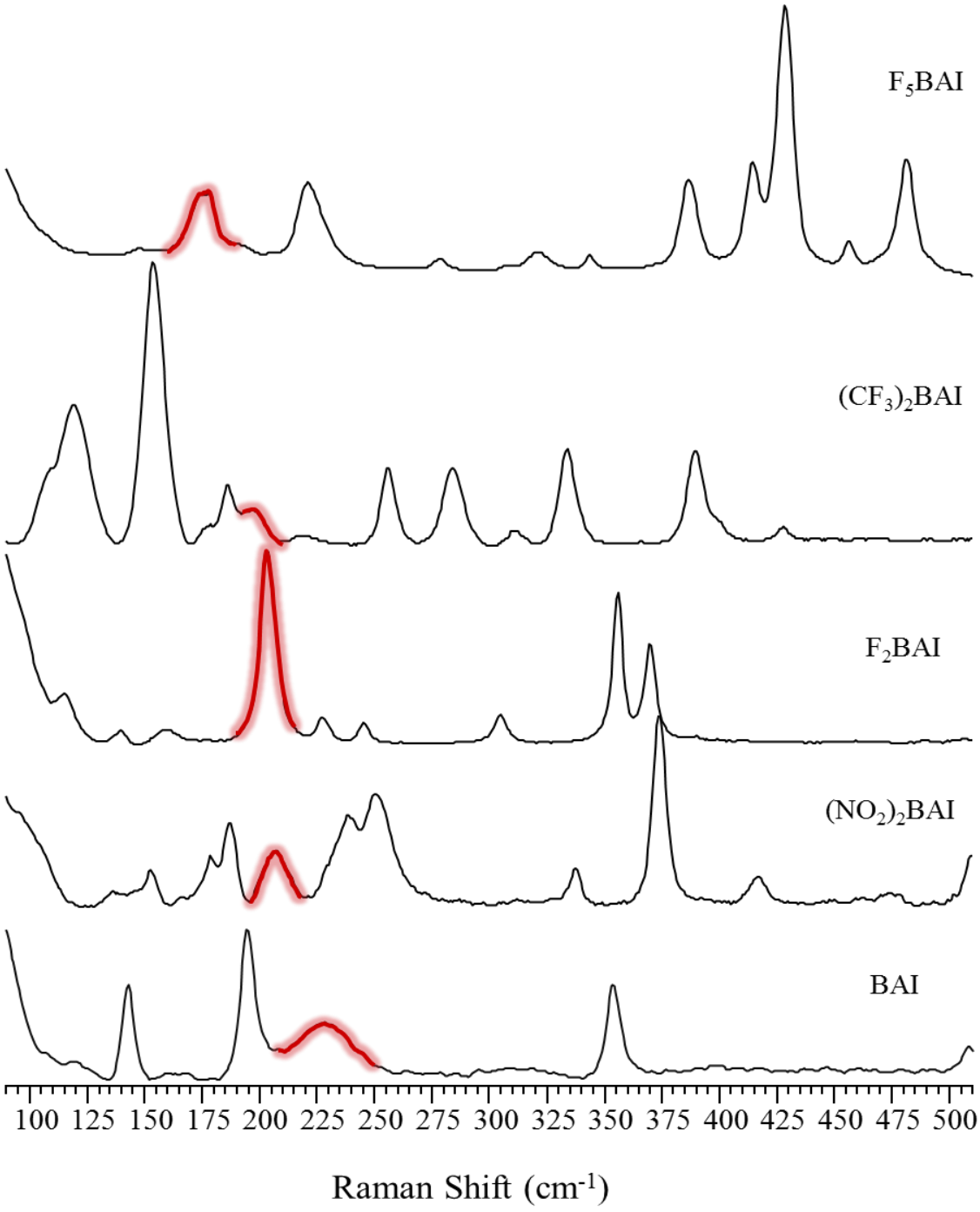

Figure 6.3.2:Trend in the C-I Stretch Observed in the Raman Spectra for Iodobenzene Derivatives

6.4 Hybridization Effects

In addition, the frequency of the C-I stretch was analyzed as a function of the hybridization of the carbon involved in the C-I bond. In conjunction with previous results, a red shift in the C-I stretch was observed as the sp^2 hybridization of the carbon in the iodobenzene derivatives was changed to the *sp* hybridization of the corresponding carbon in the (iodoethynyl)benzene derivatives. Consequently, the larger *s* character of the *sp* hybridized carbon results in a larger σ-hole on the halogen and ultimately a stronger halogen bond. The magnitude of the red shifts observed with a change in the hybridization of the carbon can be seen in Table 6.3.1 as the Δ C-I stretch.

Table 6.4.1 Hybridization Effects on C-I Stretch Frequency. All energies are in cm^{-1}.

sp^2 XB Donor	C-I stretch	*sp* XB Donor	C-I stretch	Δ C-I stretch
F_5BI	205.07	F_5BAI	178.47	-26.60
$(CF_3)_2BI$	219.50	$(CF_3)_2BAI$	197.86	-21.64
F_2BI	230.05	F_2BAI	207.22	-22.83
$(NO_2)_2BI$*	240.50	$(NO_2)_2BAI$*	203.22	-37.28
BI	266.58	BAI	238.24	-28.34

In agreement with previous works, these results concluded that the hybridization of the carbon in the C-I stretch plays a key role in halogen bond formation and strength.[11,17]

Chapter 7: Co-Crystal Results and Discussion

Here, the Raman spectra of four iodobenzene co-crystals and eight (iodoethynyl)benzene co-crystals seen in Figure 5.2.1 are presented with a focus on the C-I stretching frequency as a method for relative quantification of halogen bond interaction strengths. Only co-crystals complexing the iodobenzene halogen bond donor derivatives $(NO_2)_2$BI and F_5BI with halogen bond acceptors thiophene and furan formed and thus make up the four iodobenzene co-crystals. Co-crystals complexing the (iodoethynyl)benzene halogen bond donor derivatives $(NO_2)_2$BAI, F_2BAI, $(CF_3)_2$BAI, and F_5BAI with halogen bond acceptors thiophene and furan form and thus account for the eight (iodoethynyl)benzene co-crystals. To ensure the formation of a halogen bond within each of these co-crystals, the co-crystals were analyzed by an X-ray crystallographer and all co-crystal structures except for $(CF_3)_2$BAI/PyrT_2 were confirmed to have halogen bonding.

7.1 Trend in the C-I Stretch of Complexed Iodobenzene Derivatives

Comparison of the Raman spectra with the theoretically computed frequency of the C-I stretch for the four iodobenzene co-crystals formed aided in confident assignment of the C-I stretch in each experimental Raman spectra. Figure 7.1.1 illustrates the agreement seen between the experimental spectra and the theoretically calculated Raman frequencies

for the co-crystal $(NO_2)_2$BI/PyTF. Additionally, the experimental and theoretical frequencies of the C-I stretch in each iodobenzene co-crystal are reported in Table 7.1.1.

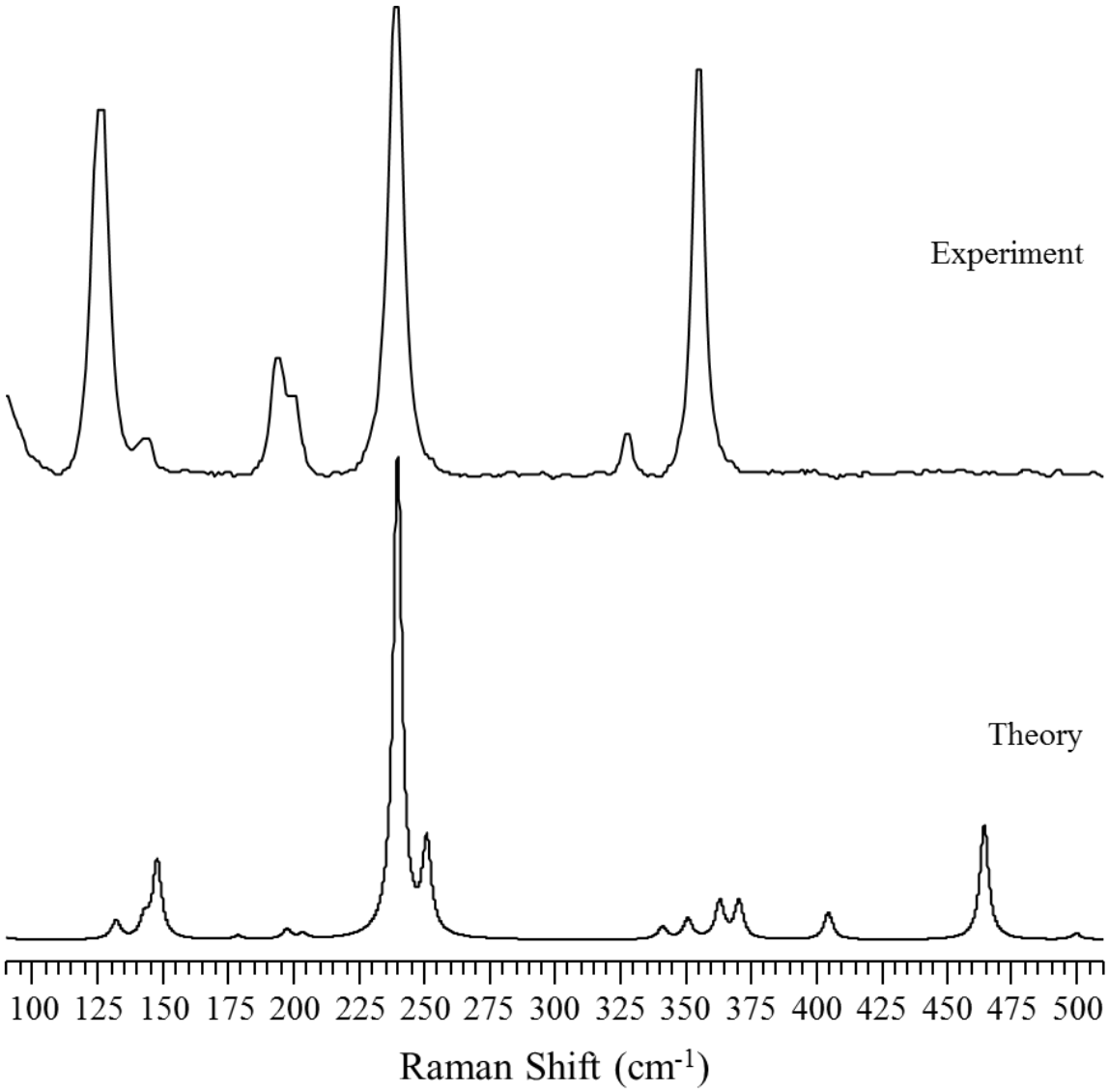

Figure 7.1.1: Agreement between the Experimental Raman and Theoretical Spectra of the C-I Stretch for the Co-crystal $(NO_2)_2$BI/PyTF.

Table 7.1.1: Experimental and Theoretical Frequencies of the C-I Stretch in Iodobenzene Derivative XB Donor co-crystals. All energies are in cm^{-1}.

Co-Crystal	Experiment	Theory
$(NO_2)_2$BI/PyTF	238.90	239.57
F_5BI/PyTF	197.41	198.54
$(NO_2)_2$BI/PyT2	247.83	239.61
F_5BI/PyT2	190.54	198.57

Spectral observations revealed a red shift, a shift to lower energy, in the C-I stretching mode and resulted in the following trend regardless of the halogen bond acceptor identity; $(NO_2)_2$BI < F_5BI, with the C-I stretching mode being the furthest red shifted in co-crystals formed with F_5BI. This trend is presented in Figure 7.1.2 and Figure 7.1.3 for halogen bond acceptor thiophene and furan respectively.

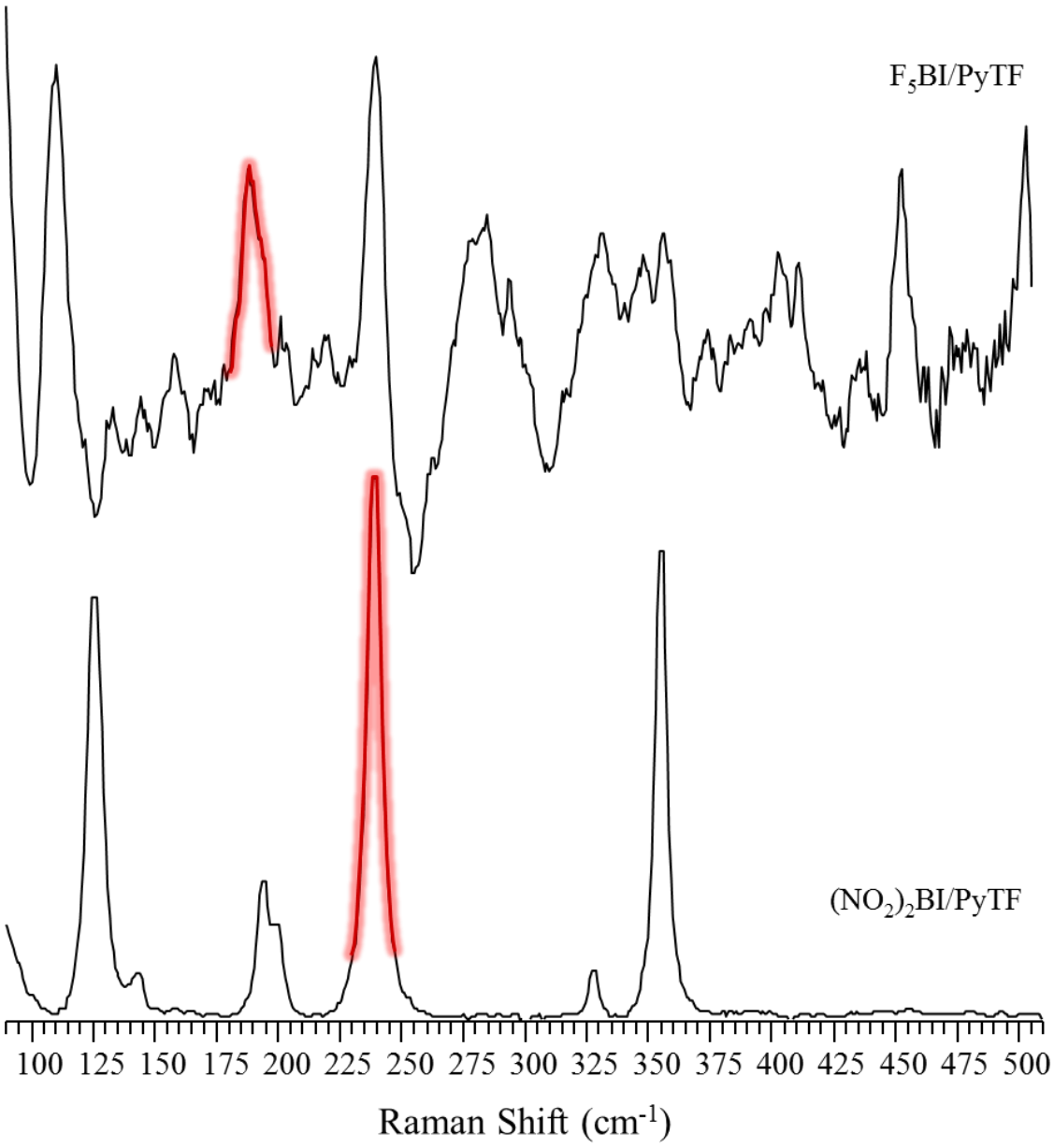

Figure 7.1.2: Trend in the C-I Stretch Observed in the Raman Spectra for Co-crystals Formed from Iodobenzene Derivatives and Thiophene

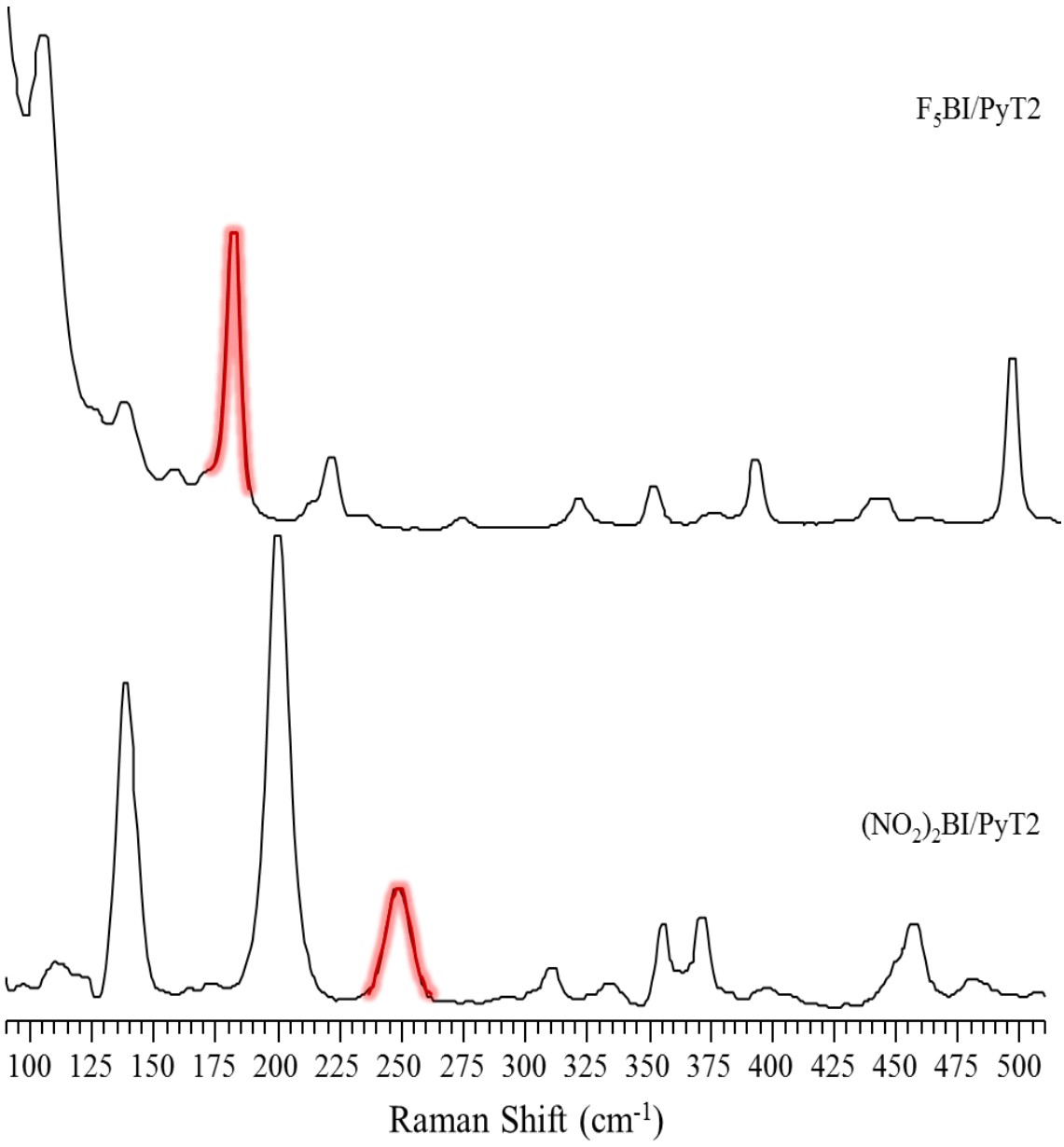

Figure 7.1.3 Trend in the C-I Stretch Observed in the Raman Spectra for Co-crystals Formed from Iodobenzene Derivatives and Furan

7.2 Δ C-I Stretch of Iodobenzene Derivatives upon Complexation

In addition to tracking the C-I stretch within each halogen bond donor and co-crystal series, the frequency of the monomeric halogen bond donor C-I stretch was compared to that of the co-crystal. Here, the location of the C-I stretches characteristic to co-crystals formed from iodobenzene derivatives and halogen bond acceptors thiophene and furan is compared to their corresponding monomeric halogen bond donors.

Table 7.2.1 ΔC-I Stretch of Iodobenzene Derivatives upon Complexation with Halogen Bond Acceptors Thiophene and Furan. All energies are in cm^{-1}.

Monomer	C-I stretch	Co-Crystal	C-I stretch	ΔC-I Stretch
$(NO_2)_2BI$	240.50	$(NO_2)_2BI/PyTF$	238.90	-1.60
F_5BI	201.35	$F_5BI/PyTF$	197.41	-7.66
$(NO_2)_2BI$	240.50	$(NO_2)_2BI/PyT_2$	247.83	7.33
F_5BI	201.35	F_5BI/PyT_2	190.54	-14.53

A substantial red shift in the frequency of the C-I stretch for both co-crystals formed with the halogen bond iodobenzene derivative F_5BI occurs regardless of the halogen bond acceptor. However, the co-crystals formed using the halogen bond iodobenzene derivative $(NO_2)_2BI$ do not demonstrate the same behavior. Rather, only the co-crystal formed with furan shows a small shift to lower energy in the C-I stretch while the C-I stretch in co-crystal formed with thiophene demonstrates a significant blue shift. These results suggest,

of the iodobenzene XB donor derivatives, F_5BI will form the strongest, most directional halogen bond.

7.3 Trend in the C-I Stretch of complexed (iodoethynyl)-benzene derivatives

Comparison of the Raman spectra with the theoretically calculated frequency of the C-I stretch for the eight (iodoethynyl)benzene co-crystals formed aided in confident assignment of the C-I stretch in each experimental Raman spectra. Figure 7.3.1 illustrates the agreement seen between the experimental spectra and the theoretically calculated Raman frequencies for the co-crystal $(NO_2)_2$BAI/PyTF.

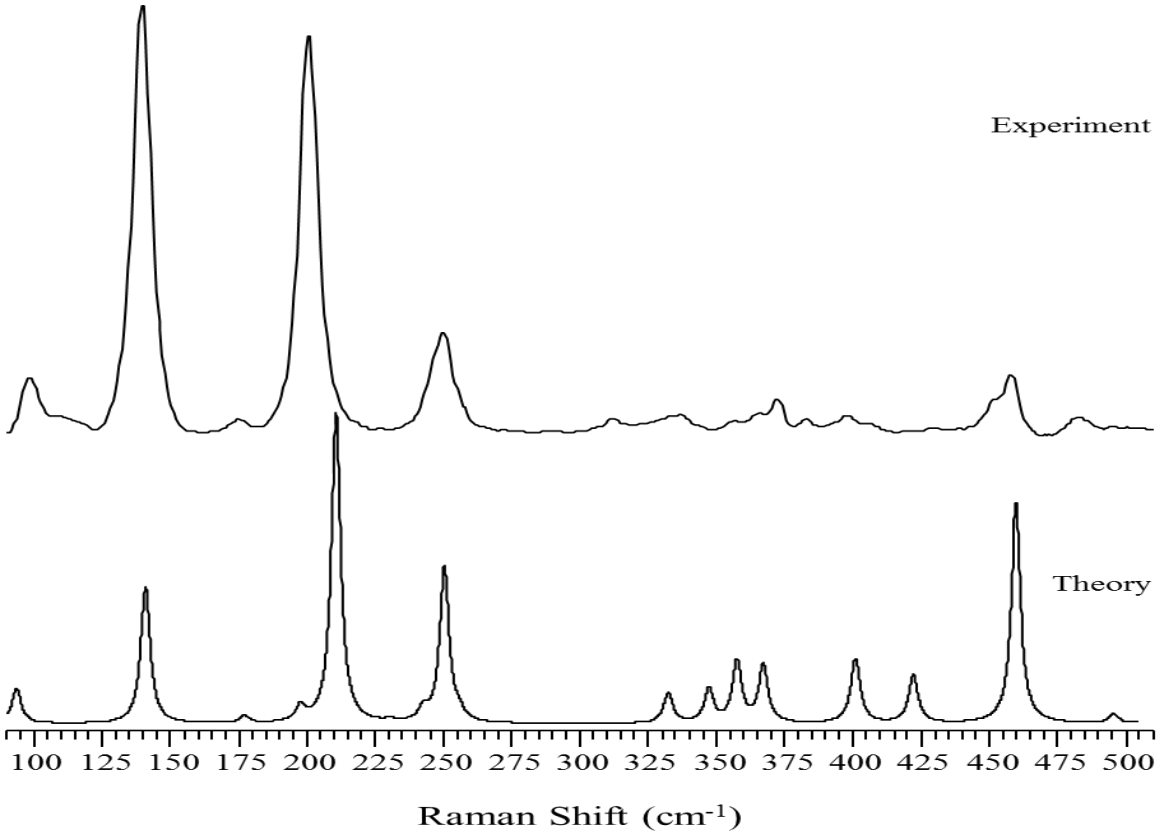

Figure 7.3.1: Agreement between the Experimental Raman and Theoretical Spectra of the C-I Stretch for the Co-crystal $(NO_2)_2$BAI/PyTF.

Additionally, the experimental and theoretical frequencies of the C-I stretch in each (iodoethynyl)benzene co-crystal are reported in Table 7.3.1.

Table 7.3.1: Experimental and Theoretical Frequencies of the C-I Stretch (Iodoethynyl)benzene Derivative XB Donor Co-crystals

	C-I Stretch (cm^{-1})	
Co-Crystal	**Experiment**	**Theory**
F_5BAI/PyTF	169.55	172.56
$(CF_3)_2$BAI/PyTF	181.50	190.24
F_2BAI/PyTF	194.91	198.22
$(NO_2)_2$BAI/PyTF	200.46	212.08
F_5BAI/PyT_2	168.92	171.78
F_2BAI/PyT_2	196.50	198.24
$(NO_2)_2$BAI/PyT_2	200.80	212.12
$(CF_3)_2$BAI/PyT_2	218.94	190.26

Spectral observations revealed a red shift, a shift to lower energy, in the C-I stretching mode and resulted in the following trends for co-crystals formed with thiophene; $(NO_2)_2$BAI < F_2BAI < $(CF_3)_2$BAI, < F_5BAI, with the C-I stretching mode being the furthest red shifted in co-crystals formed with F_5BAI. The trend in the C-I stretch for the co-crystals formed with an (iodoethynyl)benzene derivative and thiophene is presented in Figure 7.3.2.

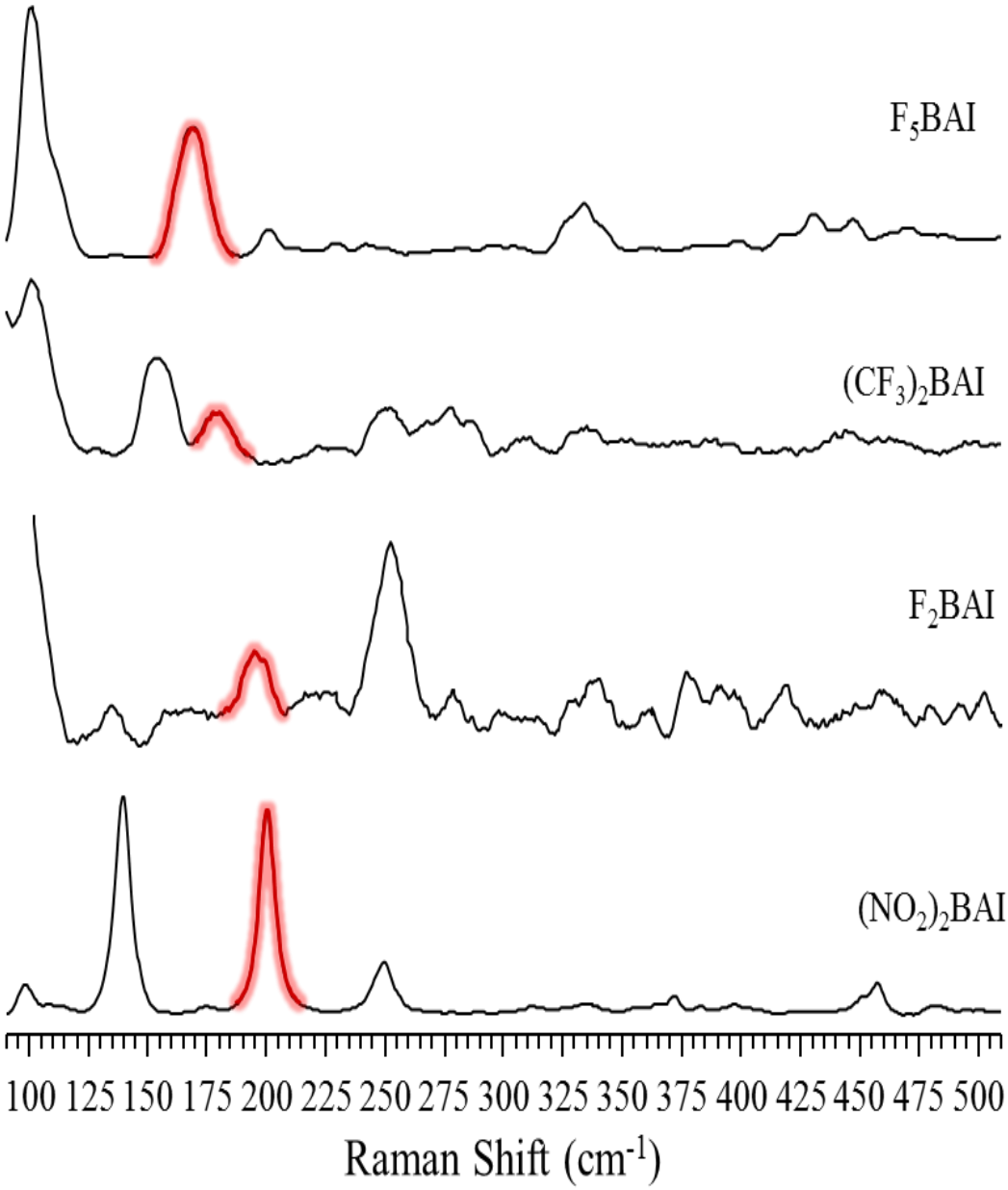

Figure 7.3.2: Trend in the C-I Stretch Observed in the Raman Spectra for Co-crystals Formed from (Iodoethynyl)benzene Derivatives and Thiophene

Surprisingly, changing the XB acceptor to furan produces a slightly different trend in that $(CF_3)_2$BAI, < $(NO_2)_2$BAI < F_2BAI < F_5BAI in that C-I stretch of $(CF_3)_2$BAI is now of the lowest energy rather than $(NO_2)_2$BAI. However, because the crystal structure was not obtained, the origin of the deficiency in halogen bond strength remains unknown. With

that said, the trend in the red shift of the C-I stretch for other co-crystals formed from an (iodoethynyl)benzene derivative and furan follows that of those formed with a thiophene acceptor. Figure 7.3.3 illustrates the trend in the C-I stretch seen for the co-crystals formed with a furan acceptor.

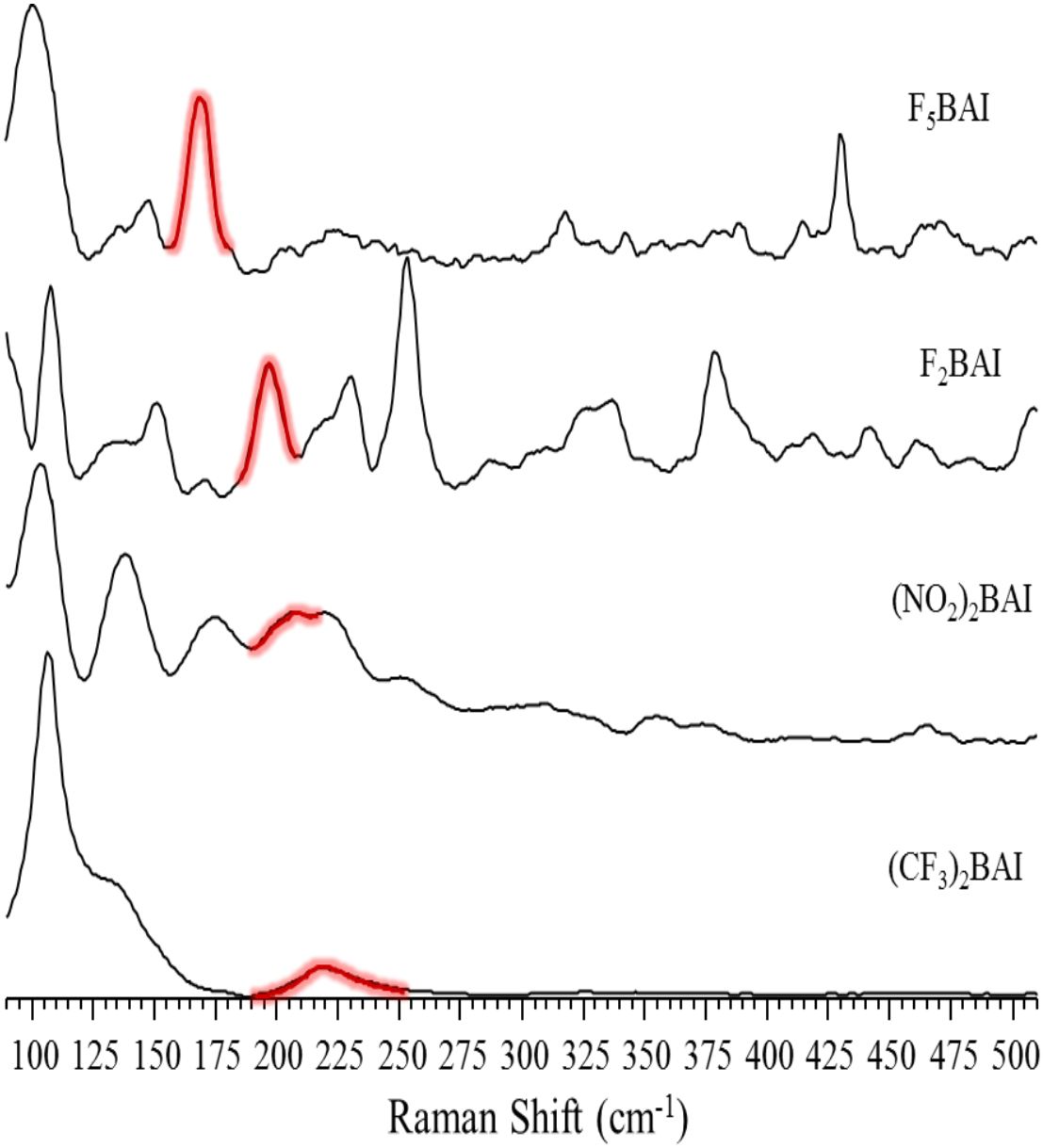

Figure 7.3.3 Trend in the C-I Stretch seen in the Raman Spectra for co-crystals formed from (iodoethynyl)benzene derivative and furan

7.4 ΔC-I Stretch of (iodoethynyl)benzene derivatives upon complexation

Here, the C-I stretches of the co-crystals formed from (iodoethynyl)benzene derivatives and acceptors thiophene and furan are compared to those of the corresponding monomeric halogen bond donor. Table 7.4.1 illustrates how the C-I stretch is affected upon complexation of an (iodoethynyl)benzene derivative XB donor with thiophene. Unexpectedly, these results suggest the strength of the halogen bond increases from $(NO_2)_2$BAI < F_5BAI < F_2BAI < $(CF_3)_2$BAI.

Table 7.4.1 ΔC-I Stretch of (Iodoethynyl)benzene Derivatives upon Complexation with Halogen Bond Acceptor Thiophene. All energies are in cm^{-1}.

Monomer	C-I stretch	Co-Crystal	C-I stretch	Δ C-I stretch
F_5BAI	178.47	F_5BAI/PyTF	169.55	-8.92
$(CF_3)_2$BAI	197.86	$(CF_3)_2$BAI/PyTF	181.50	-16.36
$(NO_2)_2$BAI*	203.22	$(NO_2)_2$BAI/PyTF	200.46	-2.76
F_2BAI	207.22	F_2BAI/PyTF	194.91	-12.31

Furthermore, Table 7.4.2 illustrates how the C-I stretch is affected upon complexation of an (iodoethynyl)benzene derivative XB donor with furan. Not surprisingly, comparing the the C-I stretch of the monomeric (iodoethynyl)benzene derivative XB donor with that of the corresponding co-crystal formed with furan as the acceptor, gives different results than those of the co-crystal formed with thiophene as the acceptor. Instead, halogen bond strength is suggested to increase from $(NO_2)_2$BAI < F_5BAI ≈ F_2BAI. The $(CF_3)_2$BAI derivative was omitted from the aforementioned ranking due to the uncertainty involved in identifying a XB by the crystallographer.

Table 7.4.2 ΔC-I Stretch of (Iodoethynyl)benzene Derivatives upon Complexation with Halogen Bond Acceptor Furan. All energies are in cm^{-1}.

Monomer	C-I stretch	Co-Crystal	C-I stretch	Δ C-I stretch
F_5BAI	178.47	F_5BAI/PyT_2	168.92	-9.55
$(CF_3)_2BAI$	197.86	$(CF_3)_2BAI/PyT_2$	218.94	21.08
$(NO_2)_2BAI$*	203.22	$(NO_2)_2BAI/PyT_2$	200.80	-2.42
F_2BAI	207.22	F_2BAI/PyT_2	196.50	-10.72

Chapter 8: Conclusions

The principal findings of this project demonstrated the complexity of designing molecular building blocks for self-assembly supramolecular materials and optoelectronic devices, implying an intricate equilibrium exists between the strength of the electron withdrawing moieties, the magnitude of the electropositive σ-hole, and the concentrated belt of electron density surrounding the halogen atom. Consequently, a simple cookie-cutter approach for the design and characterization of halogen bond donors will not accurately predict observable molecular behavior. Rather, a number of factors such as electron delocalization across the halogen bond donor upon complexation, secondary interaction competition, and the ability to accept electron density along with numerous others must be taken into account in order to get a more accurate description and understanding of the molecule's behavior. In other words, it has been experimentally and theoretically observed in this work that the σ-hole on the halogen acts as a critical factor in halogen bond formation; however, the signature vibrational characteristics of halogen bond formation previously attributed to the magnitude of the electropositive σ-hole were not observed. Therefore, another structural feature must have a profound effect on the vibrational characterization of the halogen bond. Here, it is suggested the concentrated belt of electron density surrounding the halogen atom is responsible for the unexpected spectroscopic results and ultimately has a much larger impact on halogen bond formation and vibrational characterization than previously thought.

References

(1) Tro, N. J. *Chemistry: A Molecular Approach*; Pearson Prentice Hall, 2011.
(2) Müller-Dethlefs, K.; Hobza, P. *Chemical Reviews* **2000**, *100*, 143.
(3) Shields, Z. P.; Murray, J. S.; Politzer, P. *International Journal of Quantum Chemistry* **2010**, *110*, 2823.
(4) Rowe, R. K.; Ho, P. S. *Acta Crystallographica Section B* **2017**, *73*, 255.
(5) Wang, C.; Danovich, D.; Shaik, S.; Mo, Y. *Journal of Chemical Theory and Computation* **2017**, *13*, 1626.
(6) Corradi, E.; Meille, S. V.; Messina, M. T.; Metrangolo, P.; Resnati, G. *Angewandte Chemie* **2000**, *112*, 1852.
(7) Pimentel, G. C.; McClellan, A. L. *The Hydrogen Bond [by] George C. Pimentel [and] Aubrey L. McClellan*; W.H. Freeman, 1960.
(8) Hobza, P.; Havlas, Z. *Chemical Reviews* **2000**, *100*, 4253.
(9) Arunan, E.; Desiraju, G. R.; Klein, R. A.; Sadlej, J.; Scheiner, S.; Alkorta, I.; Clary, D. C.; Crabtree, R. H.; Dannenberg, J. J.; Hobza, P. *Pure and applied chemistry* **2011**, *83*, 1637.
(10) Howard, A. A.; Tschumper, G. S.; Hammer, N. I. *The Journal of Physical Chemistry A* **2010**, *114*, 6803.
(11) Cavallo, G.; Metrangolo, P.; Milani, R.; Pilati, T.; Priimagi, A.; Resnati, G.; Terraneo, G. *Chemical Reviews* **2016**, *116*, 2478.
(12) Colin, J. J.; Gaultier de Claubry, H. *Ann. Chim* **1814**, *90*, 87.
(13) Guthrie, F. *Journal of the Chemical Society* **1863**, *16*, 239.
(14) Remsen, I.; Norris, J. *Am Chem J* **1896**, *18*, 90.
(15) Benesi, H. A.; Hildebrand, J. H. *Journal of the American Chemical Society* **1949**, *71*, 2703.
(16) Zingaro, R. A.; Hedges, R. M. *The Journal of Physical Chemistry* **1961**, *65*, 1132.
(17) Metrangolo, P.; Neukirch, H.; Pilati, T.; Resnati, G. *Accounts of Chemical Research* **2005**, *38*, 386.
(18) Metrangolo, P.; Pilati, T.; Resnati, G. *CrystEngComm* **2006**, *8*, 946.
(19) Brinck, T.; Murray, J. S.; Politzer, P. *International Journal of Quantum Chemistry* **1992**, *44*, 57.
(20) Riley, K. E.; Murray, J. S.; Fanfrlík, J.; Řezáč, J.; Solá, R. J.; Concha, M. C.; Ramos, F. M.; Politzer, P. *Journal of Molecular Modeling* **2011**, *17*, 3309.
(21) Politzer, P.; Murray, J. S.; Clark, T. *Physical Chemistry Chemical Physics* **2010**, *12*, 7748.
(22) Desiraju, G. R.; Ho, P. S.; Kloo, L.; Legon, A. C.; Marquardt, R.; Metrangolo, P.; Politzer, P.; Resnati, G.; Rissanen, K. *Pure and applied chemistry* **2013**, *85*, 1711.
(23) Lommerse, J. P. M.; Stone, A. J.; Taylor, R.; Allen, F. H. *Journal of the American Chemical Society* **1996**, *118*, 3108.
(24) Murray, J. S.; Riley, K. E.; Politzer, P.; Clark, T. *Australian Journal of Chemistry* **2010**, *63*, 1598.
(25) Clark, T.; Hennemann, M.; Murray, J. S.; Politzer, P. *Journal of Molecular Modeling* **2007**, *13*, 291.

(26) Riley, K. E.; Murray, J. S.; Fanfrlík, J.; Řezáč, J.; Solá, R. J.; Concha, M. C.; Ramos, F. M.; Politzer, P. *Journal of Molecular Modeling* **2013**, *19*, 4651.
(27) Aakeröy, C. B.; Baldrighi, M.; Desper, J.; Metrangolo, P.; Resnati, G. *Chemistry–A European Journal* **2013**, *19*, 16240.
(28) Wright, A. M.; Howard, A. A.; Howard, J. C.; Tschumper, G. S.; Hammer, N. I. *The Journal of Physical Chemistry A* **2013**, *117*, 5435.
(29) Ellington, T. L.; Reves, P. L.; Simms, B. L.; Wilson, J. L.; Watkins, D. L.; Tschumper, G. S.; Hammer, N. I. *ChemPhysChem* **2017**, n/a.
(30) Resnati, G.; Boldyreva, E.; Bombicz, P.; Kawano, M. *IUCrJ* **2015**, *2*, 675.
(31) Mayerhöffer, U.; Würthner, F. *Angewandte Chemie International Edition* **2012**, *51*, 5615.
(32) Vasylyeva, V.; Catalano, L.; Nervi, C.; Gobetto, R.; Metrangolo, P.; Resnati, G. *CrystEngComm* **2016**, *18*, 2247.
(33) Engel, T.; Reid, P. J.; Hehre, W. *Physical Chemistry*; Pearson, 2013.
(34) Straughan, B. P.; Walker, S. *Spectroscopy*; Chapman and Hall, 1976.
(35) McHale, J. L. *Molecular Spectroscopy*; Pearson Education, 2008.
(36) Struve, W. S. *Fundamentals of Molecular Spectroscopy*; Wiley, 1989.
(37) Oliveira, V.; Kraka, E.; Cremer, D. *Inorganic Chemistry* **2017**, *56*, 488.
(38) Granger, R.; Yochum, H.; Sienerth, K.; Granger, J. *Instrumental Analysis*; Oxford University Press, 2016.
(39) Ferraro, J. R. *Introductory Raman Spectroscopy*; Elsevier Science, 2003.
(40) McCreery, R. L. *Raman Spectroscopy for Chemical Analysis*; Wiley, 2005.
(41) Palmer, C. A.; Loewen, E. G. *Diffraction grating handbook*; Newport Corporation New York, 2005.
(42) Murray, J. S.; Concha, M. C.; Lane, P.; Hobza, P.; Politzer, P. *Journal of Molecular Modeling* **2008**, *14*, 699.
(43) Metrangolo, P.; Resnati, G. *Chemistry – A European Journal* **2001**, *7*, 2511.
(44) Metrangolo, P.; Resnati, G.; Pilati, T.; Liantonio, R.; Meyer, F. *Journal of Polymer Science Part A: Polymer Chemistry* **2007**, *45*, 1.